



**Calhoun: The NPS Institutional Archive**  
**DSpace Repository**

---

Theses and Dissertations

1. Thesis and Dissertation Collection, all items

---

2006-03

Enhancement of the daytime MODIS based  
aircraft icing potential algorithm using  
mesoscale model data

Cooper, Michael J.

Monterey, California. Naval Postgraduate School

---

<http://hdl.handle.net/10945/2896>

---

*Downloaded from NPS Archive: Calhoun*



Calhoun is the Naval Postgraduate School's public access digital repository for research materials and institutional publications created by the NPS community. Calhoun is named for Professor of Mathematics Guy K. Calhoun, NPS's first appointed -- and published -- scholarly author.

**Dudley Knox Library / Naval Postgraduate School**  
**411 Dyer Road / 1 University Circle**  
**Monterey, California USA 93943**

<http://www.nps.edu/library>



# NAVAL POSTGRADUATE SCHOOL

MONTEREY, CALIFORNIA

## THESIS

**ENHANCEMENT OF THE DAYTIME MODIS BASED  
AIRCRAFT ICING POTENTIAL ALGORITHM USING  
MESOSCALE MODEL DATA**

by

Michael James Cooper

March 2006

Thesis Advisor:  
Second Reader:

Philip Durkee  
Carlyle Wash

**Approved for public release; distribution is unlimited**

THIS PAGE INTENTIONALLY LEFT BLANK

REPORT DOCUMENTATION PAGE			Form Approved OMB No. 0704-0188	
Public reporting burden for this collection of information is estimated to average 1 hour per response, including the time for reviewing instruction, searching existing data sources, gathering and maintaining the data needed, and completing and reviewing the collection of information. Send comments regarding this burden estimate or any other aspect of this collection of information, including suggestions for reducing this burden, to Washington headquarters Services, Directorate for Information Operations and Reports, 1215 Jefferson Davis Highway, Suite 1204, Arlington, VA 22202-4302, and to the Office of Management and Budget, Paperwork Reduction Project (0704-0188) Washington DC 20503.				
1. AGENCY USE ONLY (Leave blank)		2. REPORT DATE March 2006	3. REPORT TYPE AND DATES COVERED Master's Thesis	
4. TITLE AND SUBTITLE: Enhancement of the Daytime MODIS Based Aircraft Icing Potential Algorithm Using Mesoscale Model Data			5. FUNDING NUMBERS	
6. AUTHOR(S) Michael J. Cooper				
7. PERFORMING ORGANIZATION NAME(S) AND ADDRESS(ES) Naval Postgraduate School Monterey, CA 93943-5000			8. PERFORMING ORGANIZATION REPORT NUMBER	
9. SPONSORING /MONITORING AGENCY NAME(S) AND ADDRESS(ES) N/A			10. SPONSORING/MONITORING AGENCY REPORT NUMBER	
11. SUPPLEMENTARY NOTES The views expressed in this thesis are those of the author and do not reflect the official policy or position of the Department of Defense or the U.S. Government.				
12a. DISTRIBUTION / AVAILABILITY STATEMENT Approved for public release; distribution is unlimited.			12b. DISTRIBUTION CODE	
13. ABSTRACT (maximum 200 words) In this thesis, MM5 mesoscale model data are examined to determine its utility in enhancing satellite based aircraft icing analysis. The algorithm by Alexander (2005) was used to process MODIS imagery on four separate storms in January 2006, and his algorithm was validated using 133 positive and negative pilot reports (PIREPs). MM5 mesoscale model soundings were then analyzed to determine the temperature (T) and dewpoint temperature (Td) at the altitude and location of each PIREP. Relative humidity (RH) was calculated, and fuzzy logic used to determine the aircraft icing potential associated with the T and RH model based parameters through the use of operational Current Icing Potential (CIP) T and RH interest maps, and the T interest map used in Alexander's algorithm. Model icing potential was calculated using 16 different methods, and it was found that weighting RH more in the calculation added the most value to the MODIS based algorithm. It was also found that the Alexander's T interest map added value to the MODIS based algorithm in every case, while the CIP based T interest map only added value when RH was weighted higher.				
14. SUBJECT TERMS MODIS, aircraft icing, multispectral satellite analysis, MM5 Model, pilot report validation			15. NUMBER OF PAGES 69	
			16. PRICE CODE	
17. SECURITY CLASSIFICATION OF REPORT Unclassified	18. SECURITY CLASSIFICATION OF THIS PAGE Unclassified	19. SECURITY CLASSIFICATION OF ABSTRACT Unclassified	20. LIMITATION OF ABSTRACT UL	

NSN 7540-01-280-5500

Standard Form 298 (Rev. 2-89)  
Prescribed by ANSI Std. Z39-18

THIS PAGE INTENTIONALLY LEFT BLANK

**Approved for public release; distribution is unlimited.**

**ENHANCEMENT OF THE DAYTIME MODIS BASED AIRCRAFT  
ICING POTENTIAL ALGORITHM USING MESOSCALE MODEL  
DATA**

Michael J. Cooper  
Lieutenant Commander, United States Navy  
B.S., United States Naval Academy, 1996

Submitted in partial fulfillment of the  
requirements for the degree of

**MASTER OF SCIENCE IN PHYSICAL OCEANOGRAPHY AND  
METEOROLOGY**

from the

**NAVAL POSTGRADUATE SCHOOL  
March 2006**

Author: Michael J. Cooper

Approved by: Philip A. Durkee  
Thesis Advisor

Carlyle Wash  
Second Reader/Co-Advisor

Philip A. Durkee  
Chairman, Department of Meteorology

THIS PAGE INTENTIONALLY LEFT BLANK

## **ABSTRACT**

In this thesis, MM5 mesoscale model data are examined to determine its utility in enhancing satellite-based aircraft icing analysis. The algorithm by Alexander (2005) was used to process MODIS imagery on four separate storms in January 2006, and his algorithm was validated using 133 positive and negative pilot reports (PIREPs). MM5 mesoscale model soundings were then analyzed to determine the temperature (T) and dewpoint temperature (Td) at the altitude and location of each PIREP. Relative humidity (RH) was calculated, and fuzzy logic used to determine the aircraft icing potential associated with the T and RH model based parameters through the use of operational Current Icing Potential (CIP) T and RH interest maps, and the T interest map used in Alexander's algorithm. Model icing potential was calculated using 16 different methods, and it was found that weighting RH more in the calculation added the most value to the MODIS based algorithm. It was also found that the Alexander's T interest map added value to the MODIS based algorithm in every case, while the CIP based T interest map only added value when RH was weighted higher.



THIS PAGE INTENTIONALLY LEFT BLANK

# TABLE OF CONTENTS

<b>I.</b>	<b>INTRODUCTION.....</b>	<b>1</b>
	<b>A. BACKGROUND.....</b>	<b>1</b>
	<b>B. MOTIVATION.....</b>	<b>4</b>
	<b>C. PURPOSE.....</b>	<b>6</b>
	<b>D. THESIS PLAN.....</b>	<b>7</b>
<b>II.</b>	<b>THEORY.....</b>	<b>9</b>
	<b>A. MODEL BASED ICING POTENTIAL PREDICTION.....</b>	<b>9</b>
	<b>B. MODIS BASED ICING POTENTIAL ALGORITHM.....</b>	<b>11</b>
	<b>1. Group I Reflectance tests.....</b>	<b>12</b>
	<i>a. P01 Reflectance Test.....</i>	<i>13</i>
	<i>b. P06 Reflectance Test.....</i>	<i>14</i>
	<i>c. P07 Reflectance Test.....</i>	<i>16</i>
	<i>d. P22 Reflectance Test.....</i>	<i>16</i>
	<i>e. P26 Reflectance Test.....</i>	<i>17</i>
	<b>2. Group II Reflectance Ratio Tests: P61 and P71.....</b>	<b>18</b>
	<b>3. Group III Brightness Temperature Test (P31).....</b>	<b>20</b>
	<b>4. Group IV Brightness Temperature Difference Tests.....</b>	<b>20</b>
	<i>a. BTD1 Brightness Temperature Difference Test.....</i>	<i>21</i>
	<i>b. BTD2 Brightness Temperature Difference Test.....</i>	<i>22</i>
	<i>c. BTD3 Brightness Temperature Difference Test.....</i>	<i>22</i>
	<i>d. BTD4 Trispectral Brightness Temperature Difference Test.....</i>	<i>23</i>
	<b>5. The Final MODIS Algorithm Test.....</b>	<b>24</b>
<b>III.</b>	<b>PROCEDURE.....</b>	<b>27</b>
	<b>A. RAW MODIS FILE INVESTIGATION.....</b>	<b>27</b>
	<b>B. MM5 MODEL DATA INVESTIGATION.....</b>	<b>27</b>
	<b>C. TOTAL ICING POTENTIAL CALCULATIONS.....</b>	<b>29</b>
	<b>1. Model Icing Potential Assignment.....</b>	<b>29</b>
	<i>a. RH Icing Potential Assignment.....</i>	<i>29</i>
	<i>b. T Icing Potential Assignment.....</i>	<i>29</i>
	<b>2. Eight Test Calculations.....</b>	<b>29</b>
	<i>a. MM5_1.....</i>	<i>30</i>
	<i>b. MM5_2.....</i>	<i>30</i>
	<i>c. MM5_1_1.....</i>	<i>30</i>
	<i>d. MM5_2_1.....</i>	<i>32</i>
	<i>e. MM5_1_2.....</i>	<i>32</i>
	<i>f. MM5_2_2.....</i>	<i>32</i>
	<i>g. MM5_3.....</i>	<i>32</i>
	<i>h. MM5_4.....</i>	<i>33</i>
	<b>D. VERIFICATION.....</b>	<b>33</b>

<b>IV.</b>	<b>RESULTS .....</b>	<b>35</b>
<b>A.</b>	<b>RAW MODIS FILE INVESTGATION RESULTS AND MODIS ICING POTENTIAL RESULTS .....</b>	<b>35</b>
<b>B.</b>	<b>MODEL ICING POTENTIAL CALCULATION RESULTS.....</b>	<b>38</b>
<b>1.</b>	<b>ROC Curves.....</b>	<b>40</b>
<b>V.</b>	<b>CONCLUSION AND RECOMMENDATIONS.....</b>	<b>45</b>
<b>A.</b>	<b>CONCLUSION .....</b>	<b>45</b>
<b>B.</b>	<b>RECOMMENDATIONS .....</b>	<b>46</b>
	<b>LIST OF REFERENCES.....</b>	<b>49</b>
	<b>INITIAL DISTRIBUTION LIST .....</b>	<b>53</b>

## LIST OF FIGURES

Figure 1.	Balance of forces for level flight (from <a href="http://www.grc.nasa.gov/WWW/K-12/airplane/forces.html">http://www.grc.nasa.gov/WWW/K-12/airplane/forces.html</a> )	19
	January 2006.....	2
Figure 2.	Leading edge mixed icing (from <a href="http://www.aopa.org/asf/publications/sa11.pdf">http://www.aopa.org/asf/publications/sa11.pdf</a> 19 January 2006)	3
Figure 3.	A typical depiction of a standard EHSI with a MODIS based icing potential overlay (sandel.com 2006)	6
Figure 4.	Example of the final product of Alexander's MODIS based algorithm (from Alexander 2005)	7
Figure 5.	RH interest map (after Bernstein et al 2005)	10
Figure 6.	T interest maps (from Alexander 2005 and after Bernstein et al. 2005)	11
Figure 7.	P01 icing potential vs channel 1 reflectance percentage (from Alexander 2005)	13
Figure 8.	Imaginary index of refraction between 0.5 and 2.5 $\mu m$ (Baum et al. 2000)	15
Figure 9.	P06 Icing potential vs. channel 6 reflectance percentage (from Alexander 2005)	15
Figure 10.	P07 icing potential vs. channel 7 reflectance percentage (from Alexander 2005)	16
Figure 11.	P22 icing potential vs. channel 22 reflectance percentage (from Alexander 2005)	17
Figure 12.	P26 icing potential vs. channel 26 reflectance percentage (from Alexander 2005)	18
Figure 13.	P61 Icing potential vs. P61 ratio (from Alexander 2005)	19
Figure 14.	P71 Icing potential vs. P71 ratio (from Alexander 2005)	19
Figure 15.	P31 Brightness Temperature probability values (from Alexander 2005)	20
Figure 16.	BTD1 icing potential vs Channel 22-31 brightness temperature difference (from Alexander 2005)	21
Figure 17.	BTD2 icing potential vs. channel 29-32 brightness temperature difference (from Alexander 2005)	22
Figure 18.	BTD3 icing potential vs. channel 31-32 brightness temperature difference (from Alexander 2005)	23
Figure 19.	BTD4 icing potential vs. trispectral brightness temperature difference (from Alexander 2005)	24
Figure 20.	Illustration of the final aircraft icing potential test (Alexander 2005)	25
Figure 21.	Sample GARP model sounding output	28
Figure 22.	Raw January 23, 2006 channel 6 reflectance field	36
Figure 23.	Filtered January 23, 2006 channel 6 reflectance field	36
Figure 24.	Channel 22 brightness temperature field from January, 15, 2006	37

Figure 25. ROC curves using 3 hour PIREPs and Alexander Tmap with symbols plotted at the 0.5 threshold values..... 42

Figure 26. ROC curves using 3 hour PIREPs and Alexander Tmap with symbols plotted at the 0.5 threshold values..... 44

## LIST OF TABLES

Table 1.	MODIS icing tests (after Alexander 2005) .....	12
Table 2.	Channel specifications for the MODIS platform (after MODIS web 2006) .....	26
Table 3.	Model icing potential calculations [table titles go at the top] .....	31
Table 4.	Results using T icing potential values from the Alexander Tmap, and 3 Hour PIREPs .....	39
Table 5.	Results using T icing potential values from the CIP Tmap, and 3 hour PIREPs.....	39
Table 6.	Important ROC variables. Plotted variables highlighted in light grey. ....	41

THIS PAGE INTENTIONALLY LEFT BLANK

## **ACKNOWLEDGMENTS**

The author would like to thank Professor Phil Durkee for his guidance during the thesis process, and Professor Chuck Wash for his review of the final product. A special thanks to Captain Brandon Alexander, USAF whose research and development of the MODIS based icing potential calculation provided the base on which this research was built. Professor Mary Jordan was a great help in troubleshooting and adapting the MATLAB programs originally developed by Dr. Shaima Nasiri , and adapted by Capt Alexander. Thanks to Kurt Nielsen for pointing the way to raw MODIS files, and Bob Creasey for collecting the AFWA MM5 model fields.

Thanks to all of my family and friends who have given me support during this process.



THIS PAGE INTENTIONALLY LEFT BLANK

# I. INTRODUCTION

## A. BACKGROUND

In-flight icing is an ever present hazard to aviation around the world. It can occur any time of the year, at any altitude, and at any latitude. Its effects are multiple, and can lead to loss of money, equipment, and life. With the International Air Transport Association forecasting that international air traffic will grow by 5.9% between 2005 and 2009 (International Air Transport Association 2004), it is apparent that a robust assessment and prediction of in-flight icing potential is essential to increased safety of flight.

Studies to assess and predict in-flight icing have increased steadily over the last decade after an American Eagle commuter flight crashed near Roselawn, Indiana on 31 October 1994. The aircraft was instructed to hold while waiting to be sequenced into Chicago O'Hare International Airport (KORD). Unknown to the air traffic controller, the aircraft was holding in, and descending through, severe icing conditions. The aircrew was aware that they were experiencing some icing, and post crash investigations revealed that they were using anti-icing equipment, but this clearly was not enough. The black box transcript of the last minutes of the flight reveals that the aircraft was on a descent to eight thousand feet when it lost control and crashed (planecrashinfo.com 2006). The aircrew members were completely calm until the point where they lost controlled flight, which indicates that the aircrew was unaware of the severity of the icing. As a result, all 68 passengers and aircrew on board were killed.

In-flight icing can occur in the atmosphere over any point on earth. The requirements are simple: the aircraft must be flying through supercooled liquid water (SLW) of any form, and the airframe must be at or below 0°C. Both criteria must be met at the same point, and time, for icing to occur. Most modern commercial and military aircraft cruise at altitudes where temperatures are below the threshold for SLW presence, but these conditions could be encountered during the climb, descent, and possible holding phases of flight. Icing poses a

more direct threat to smaller commuter, commercial, and private aircraft flown in instrument flight rules (IFR) conditions by IFR rated pilots. These aircraft generally fly at lower altitudes where the presence of SLW is more likely in the form of clouds, rain, or drizzle making the icing threat possible during all phases of flight for these aircraft.

The dynamics of flight require laminar flow over a smooth surface to achieve balanced flight. Balanced flight occurs when lift is equal and opposite to the weight of the aircraft, and thrust is equal and opposite to the drag of the aircraft. When in balanced flight, an aircraft is able to maintain a constant airspeed and altitude. This balance of forces is depicted in Figure 1.

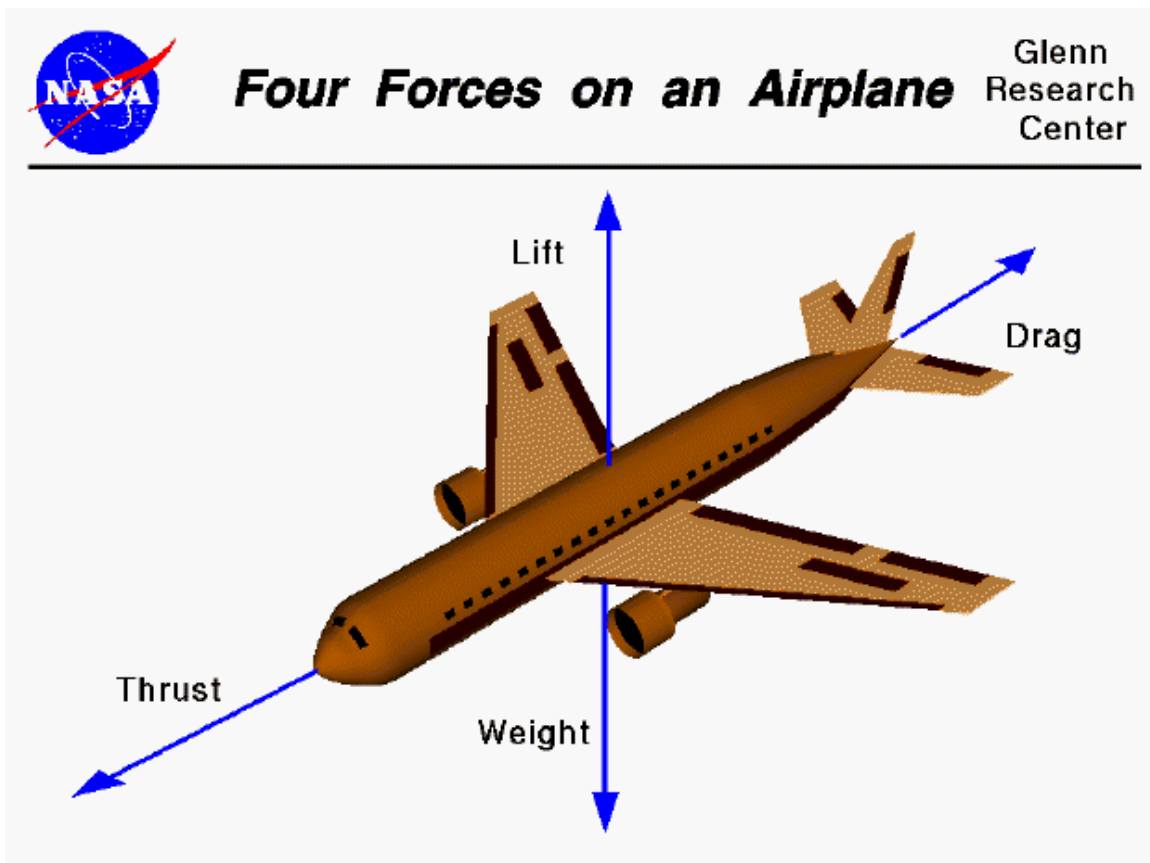


Figure 1. Balance of forces for level flight (from <http://www.grc.nasa.gov/WWW/K-12/airplane/forces.html> 19 January 2006).

The effects of icing are varied, and have the potential of becoming catastrophic. As can be seen in Figure 2, the ice that accretes on aircraft wings

is usually rough and irregular. Its physical existence acts to increase weight of the aircraft, but the more severe result comes from its coarseness. Its coarse surface increases the drag and disrupts the smooth airflow over the wings. The combined effect is that the aircraft loses lift and is no longer maintaining balanced flight. To bring the aircraft back into balanced flight the pilot must increase the angle of attack (AOA) and increase the throttle settings. This acts to produce more thrust and lift to balance the increased drag and weight produced by the ice on the airframe. Higher throttle settings mean higher fuel flows, and therefore, higher flight costs.



In-flight wing leading edge ice formation

Figure 2. Leading edge mixed icing (from <http://www.aopa.org/asf/publications/sa11.pdf> 19 January 2006)

On the more extreme end of the spectrum, in-flight icing can lead to loss of control and ultimately loss of life. Ice accretion is typically non-uniform over the entire airframe, and tends to build more rapidly on smaller airfoils like the horizontal stabilizers on the rear of the aircraft. This is known as a tail stall, and when it occurs the aircraft would pitch upward causing the wings to stall sending the aircraft into a dive. If the dive is uncontrollable a crash is inevitable. In aviation terms a stall is simply a complete loss of lift by an airfoil, and a tail stall is not the only stall threat. If ice accretes more rapidly on one of the wings it can result in asymmetrical lift or a complete stall of one wing. Both situations could possibly cause the aircraft to enter into an uncontrollable roll. There also exists the physical threat of ice binding control cables and control surfaces which could take away the pilots ability to safely maneuver the aircraft.

While the icing threat is mitigated by the proper training of pilots, not all icing situations are properly assessed by the aircrew. Severe icing can lead to the loss of the aircraft in spite of anti-icing equipment and proper training as highlighted by the American Eagle crash in 1994. The only definite method for eliminating the icing threat is to never enter icing conditions. Clearly this is not a viable solution in today's aviation industry. Aircraft must fly in IFR conditions to get passengers and freight to their destinations on time.

## **B. MOTIVATION**

Icing is clearly a threat to aviation throughout the world, and it is equally clear that this threat will not keep planes from flying. It is nearly impossible for IFR flight traffic to avoid icing completely, but it is possible to minimize the likelihood of a severe encounter. Proper prior planning on the part of the aircrew and air traffic controllers could lead to far fewer catastrophic in-flight icing incidents. At the present time there are several products available that provide a nowcast and forecast of icing potential in the atmosphere. This information typically falls under the "for your information" category, and how the information is used is at the discretion of the pilot. It is possible that airline or military policies may limit flights and into forecast icing areas, but to the instrument rated private pilot this information is precautionary.

Current methods of icing assessment and prediction include model data, satellite data, PIREP data, and products that fuse the various sources. Model fields have become more accurate over the years, but they generally predict overly broad areas where temperature and relative humidity criteria would indicate icing. Operational satellite based products are currently based on data fields from the geostationary operational environmental satellites (GOES), and are limited to providing a horizontal depiction. The effectiveness of PIREPs has been limited due to lack of coverage, detail, accuracy, and timeliness (Erickson 1997). Fused products, like the current icing potential (CIP) (Bernstein et al. 2005), incorporate multiple sources of information (model, satellite, radar, PIREPs, etc.) to more accurately portray the current icing potential.

While a great improvement over individual sources, the CIP is limited to the use of GOES data fields which are currently limited to 5 multispectral channels. Of those five channels, only 3 are used to determine icing potential. In 2005, Alexander proposed a daytime Moderate Resolution Imaging Spectroradiometer (MODIS) based algorithm to predict icing potential which improved upon the currently operational GOES based algorithm. The use of this algorithm fused with other sources of information could improve upon currently operational methods of assessing and predicting icing potential with an ultimate goal of producing a near real time icing potential product available to pilots in the cockpit.

A possible depiction of such a product can be seen in Figure 3. This depiction is typical of today's Electronic Horizontal Situation Indicators (EHSI) found in many cockpits. In this example the EHSI is overlaid with a MODIS based icing potential field. The aircraft's current position is marked by the light blue triangle, and its desired flight path is shown as a white line leading to airport KSBA. The warm colors indicate high icing potential, and cold colors indicate low icing potential. The numbers to the right of the triangle indicate the altitudes where icing potential is high. Given the situation depicted, the pilot would know that the flight path would take the plane through probable icing, and if encountered and accumulating at high rates, could likely find ice free conditions just to the south (left as depicted). While this type of product is not currently possible using the MODIS platform, future versions of the GOES imager will provide the multispectral channels and time resolution required to make this product a reality.



Figure 3. A typical depiction of a standard EHSI with a MODIS based icing potential overlay (sandel.com 2006)

### C. PURPOSE

The aim of any research attempting to more accurately depict, or predict, in-flight icing potential is to increase flight safety. The secondary benefits of icing prediction are the minimized costs associated with the elimination of unnecessary rerouting, fuel economy, and decreased maintenance. With the main goal of safety in mind, Alexander (2005) developed a MODIS based 9-channel fuzzy logic aircraft icing potential algorithm. His algorithm proved to be more accurate in predicting positive icing PIREPS than the currently operational GOES algorithm. The deficiency with the algorithm's output is the fact that it is limited to a two dimensional horizontal depiction. While beneficial, a horizontal product gives a very limited picture of icing in the atmosphere since there is also a vertical component to the icing hazard. Icing is a three dimensional phenomenon, and the purpose of this study is to assess the value of using mesoscale model data to increase the specificity of the MODIS based icing potential prediction to certain flight levels. An example of the output from Alexander's algorithm can be seen in Figure 4.

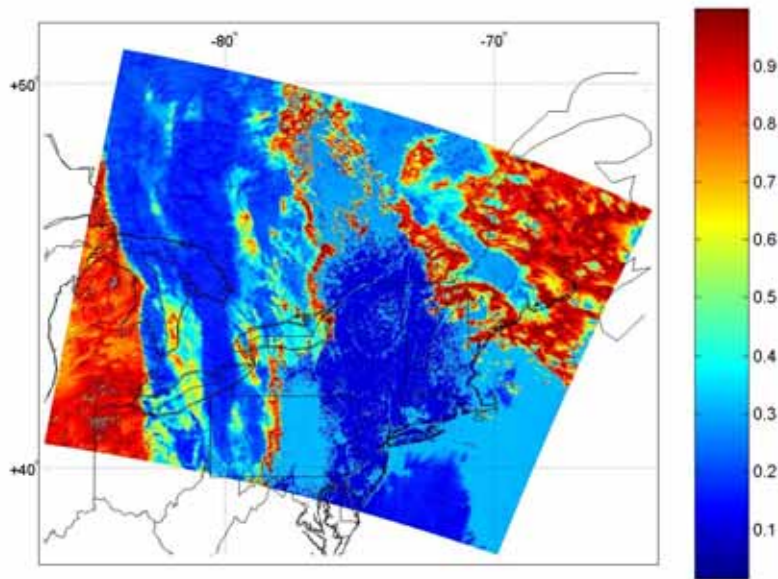


Figure 4. Example of the final product of Alexander's MODIS based algorithm (from Alexander 2005).

#### **D. THESIS PLAN**

Brandon Alexander's MODIS based fuzzy logic algorithm will be used to determine the MODIS based aircraft icing potential during several recent northeastern United States Storms. MM5 model data will then be examined to determine if its addition would make icing potential predictions at PIREP locations more accurate. Theory associated with this type of study will be discussed in Chapter II. Chapter III will explain the data collection and verification procedures. Chapter IV will explain the results, and Chapter V will close the thesis with conclusions and recommendations.



THIS PAGE INTENTIONALLY LEFT BLANK

## II. THEORY

### A. MODEL BASED ICING POTENTIAL PREDICTION

Most early icing potential prediction products were completely model-based, and almost all current icing potential prediction products have a model component. The theory is actually quite simple. The only questions that need to be answered are: where within the model volume are the clouds, and where within the clouds is the temperature conducive to icing? More detailed questions could be asked, but we only attempt to answer these two here.

The first model parameter that comes to mind when trying to answer the questions posed above is relative humidity (RH). One might expect that clouds only exist in areas where relative humidity is close to 100%, but the reality of models is that relative humidity rarely reaches 100% and it is generally accepted that clouds exist in models at relative humidities above 70%. In Thomson et al.'s (1997b) intercomparison of several earlier in-flight icing algorithms, all of the automated algorithms used RH thresholds well below 100%. The National Center for Atmospheric Research's (NCAR) Research Applications Program's (RAP) icing algorithm's minimum RH threshold was 56% and the National Aviation Weather Advisory Unit's (NAWAU) icing algorithm's minimum was 60%. In these early algorithms the RH values threshold was a hard threshold. This meant that if the RH was below the threshold no icing was predicted, and above the same threshold, icing was predicted on the condition that the temperature was in the correct range. This type of algorithm eventually gave way to a more inclusive fuzzy logic based algorithm that weights RH values in icing potential calculations.

One such algorithm is the Current Icing Potential (CIP) as described in Bernstein et al. (2005). This product is the most current, and most robust, operational icing algorithm ever developed. It uses model data as one of many inputs to help determine icing potential, and RH is only one of four model parameters examined. A RH interest map (RHmap) based on the RHmap used

in the CIP can be seen in Figure 5, and is a good example of fuzzy logic. This RHmap assigns the highest potential to high relative humidities, and the potential tapers off as RHs decrease. A close inspection reveals that significant potentials still exist down to RHs well below 100%. This more inclusive fuzzy logic based RHmap found in Figure 5 appeared to be a natural choice to compliment the fuzzy logic MODIS based icing potential algorithm, and is the RHmap used in this study.

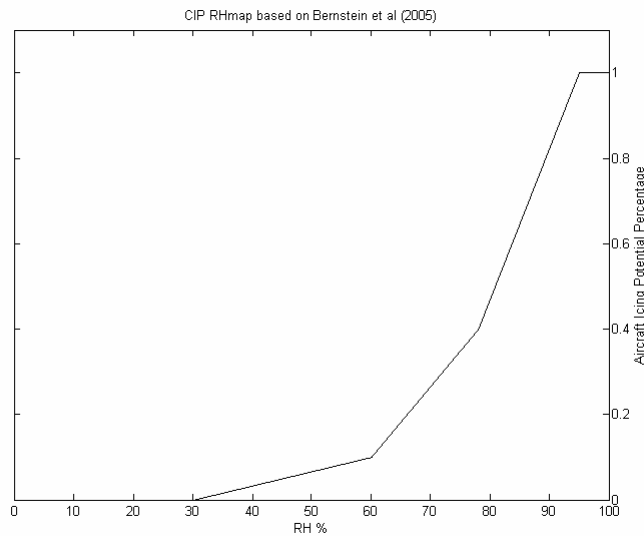


Figure 5. RH interest map (after Bernstein et al 2005)

The second model parameter needed to answer the questions posed is the Temperature (T) parameter. This parameter's importance to icing potential seems rather intuitive, but as used in this study, it is more involved than the RH contribution. Again, as discussed in Thomson et al. (1997b) and Bernstein et al. (2005), early icing algorithms used simple temperature ranges to make an icing potential determination and later algorithms migrated to a fuzzy logic methodology. Figure 6 displays both T interest maps (Tmap) used in this study. Both use a fuzzy logic method for assigning T based icing potential values. Interesting to note is the shape of these curves. SLW drops, by definition, are already at temperatures below 0 degrees Celsius, and an intensive study of 19,057 PIREPs revealed that positive icing PIREP frequencies peak near -7

degrees Celsius (Bernstein et al.2005). This fact drives the shape of both Tmaps used in this study. The Alexander Tmap was based on research conducted by Sand et al. (1984), and the CIP Tmap was based on the Tmap currently used in the CIP calculation as outlined in Bernstein et al. (2005). These Tmaps based on two separate studies both agree that icing peaks below 0 degrees Celsius and drops off as temperature decreases toward -25 degrees Celsius. Below -25 degrees Celsius SLW begins to spontaneously freeze creating an ice cloud which poses no icing threat.

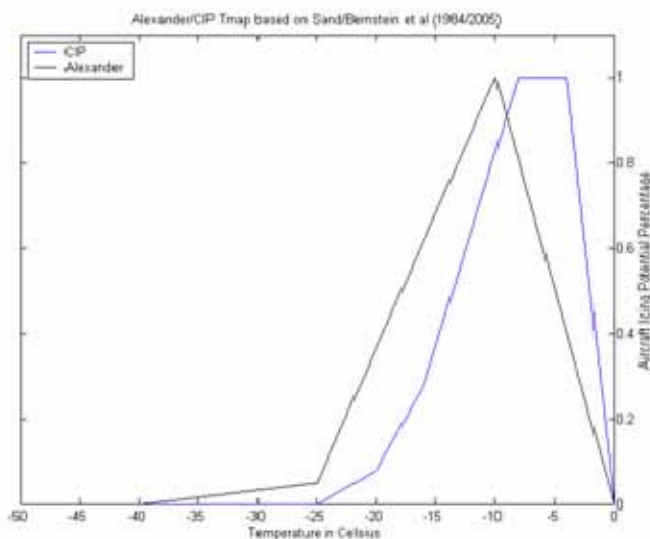


Figure 6. T interest maps (from Alexander 2005 and after Bernstein et al. 2005)

Looking at both the T and RH parameters at the same point in space and time allows for the calculation of icing potential. Alone these provide just a value, but together they can possibly predict icing conditions in a cloud. A high RH value paired with a T above 0 degrees Celsius would indicate no icing potential, the same RH value and a T at -7 degrees Celsius would indicate a high icing potential.

## B. MODIS BASED ICING POTENTIAL ALGORITHM

Alexander (2005) developed a MODIS based aircraft icing potential algorithm. His approach used 9 of the 36 available MODIS channels, and fuzzy logic to develop a robust algorithm comprised of twelve tests. Those twelve tests

are further divided into four groups. This algorithm outperformed the currently operational 3 channel GOES based method in detecting areas of positive icing PIREPs. Table 1 lists the twelve tests and four test groups developed by Alexander. Table 2 lists the 36 MODIS channels and their characteristics for reference. Each test in Alexander's algorithm will be explained followed by a figure depicting the specifics of assigning an icing potential value. What follows is a brief synopsis of each test as described in Alexander (2005).

Table 1. MODIS icing tests (after Alexander 2005)

<b>Test Group</b>	<b>Test (no units unless noted)</b>	<b>Icing Reflectance Thresholds</b>
I	0.65 $\mu$ m Reflectance (P01)	Min < 0.10 Max > 0.25
I	1.63 $\mu$ m Reflectance (P06)	> 0.5
I	2.1 $\mu$ m Reflectance (P07)	> 0.4
I	3.9 $\mu$ m Reflectance (P22)	> 0.06
I	Cirrus Reflectance (P26)	< 0.08
II	1.63 $\mu$ m Ratio (P61)	Min < 0.2 Max > 0.9
II	2.1 $\mu$ m Ratio (P71)	Min < 0.15 Max < 0.65
III	Temperature ( $^{\circ}$ C) (P31)	Min > 0 & < -40 Max @ -10
IV	3.9-11 $\mu$ m BTD ( $^{\circ}$ C) (BTD1)	> 10 (Day)
IV	8-11 $\mu$ m BTD ( $^{\circ}$ C) (BTD2)	Min > 3 Max < -2
IV	11-12 $\mu$ m BTD ( $^{\circ}$ C) (BTD3)	< -0.5 & > 4.5
IV	Trispectral BTD ( $^{\circ}$ C) (BTD4)	Same as 8-11 BTD

### 1. Group I Reflectance tests

Alexander's first group of tests are reflectance tests using MODIS channels 1 (0.65  $\mu$ m), 6 (1.6  $\mu$ m), 7 (2.1  $\mu$ m), 22 (3.9  $\mu$ m), and 26 (1.38  $\mu$ m). Reflectance tests are simply a measure of the energy that arrives at the satellites

sensors after being reflected by a surface within its field of view. While seemingly simplistic, the use of thresholds allows one to discriminate cloud from background and possible composition/phase of the cloud.

**a. P01 Reflectance Test**

The P01 test uses MODIS channel 1 ( $0.65\ \mu\text{m}$ ), which is in the middle of the visible wavelength spectrum, and is located in a spectral window where the atmosphere is nearly transparent. At this wavelength everything will reflect a certain amount of energy back into space, but optically thick clouds reflect a majority of incident visible solar energy. By measuring the amount of energy received at the sensor and correcting for sun angle it is possible to distinguish cloud from ground or ocean. There is some difficulty in distinguishing cloud from snow or desert at this wavelength, but these areas can be broken out through the use of near-infrared and temperature thresholds in other tests. For the purposes of the icing potential algorithm, Alexander set the maximum icing potential probability at the  $>.25$  reflectance values and the minimum at the  $<.10$  reflectance values with a linear relationship between the two points as depicted in Figure 7.

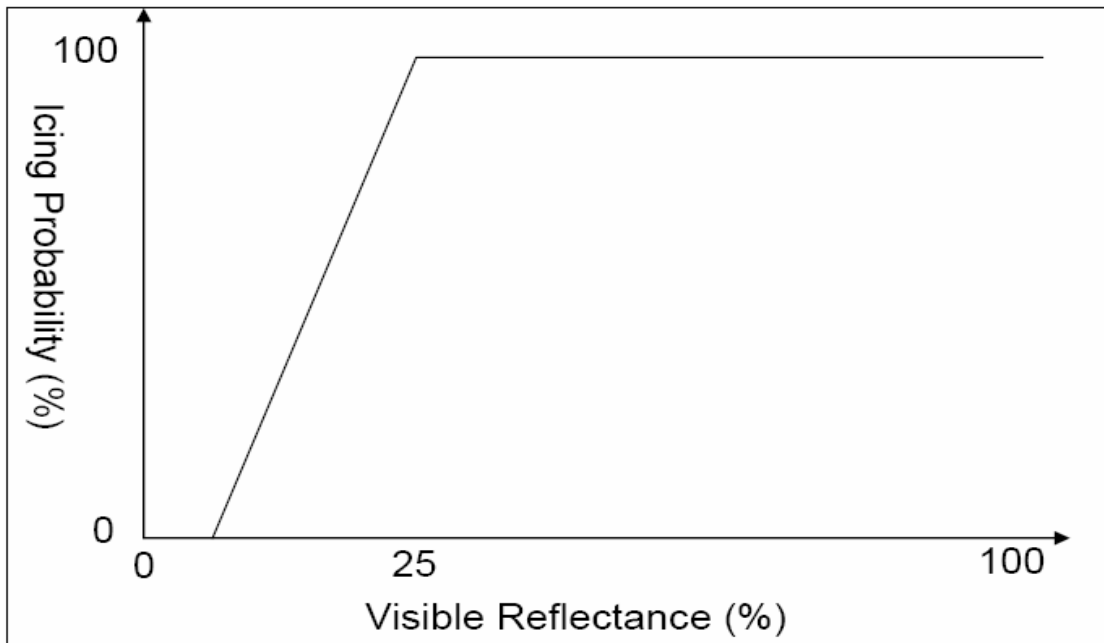


Figure 7. P01 icing potential vs channel 1 reflectance percentage (from Alexander 2005)

**b. P06 Reflectance Test**

The P06 test uses MODIS channel 6 ( $1.6 \mu m$ ), and is primarily used to determine the phase of the cloud. The P06 test is limited to daytime use and is in a portion of the solar spectrum that makes it possible to determine cloud composition. Figure 8 shows the imaginary index of refraction of clouds based on their composition which has a direct relationship with absorption. If more energy is absorbed at a certain wavelength then there is less energy reflected back to the satellite sensors. At the channel 6 wavelength ( $1.6 \mu m$ ) the real index of refraction is nearly identical for ice and water clouds, but the imaginary index of refraction is clearly unequal. The ice cloud has a much larger imaginary index of refraction, and therefore absorbs more solar energy than a water cloud. The result of this difference is that the MODIS sensor sees water clouds as brighter than ice clouds. This is helpful in determining icing potential, as icing potential increases with increasing SLW content in clouds. It should be noted that brightness of a water cloud decreases with increasing drop size, and the same occurs in an ice cloud. The decreased brightness could lead to crossover into the brightness of an ice cloud made up of small ice particles. Alexander placed the threshold for maximum icing potential at the  $>0.5$  reflectance value to mitigate the possibility of ice clouds being assigned a high icing potential. Figure 9 depicts the specifics of this test.

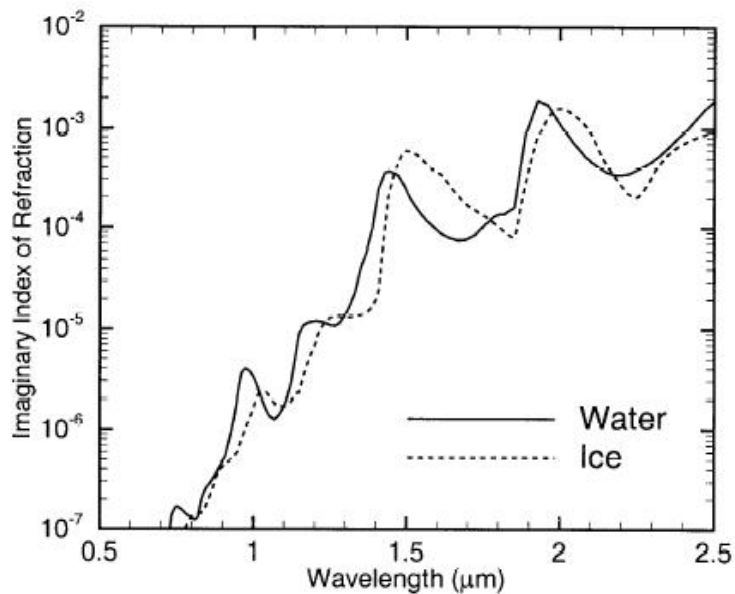


Figure 8. Imaginary index of refraction between 0.5 and 2.5  $\mu m$  (Baum et al. 2000).

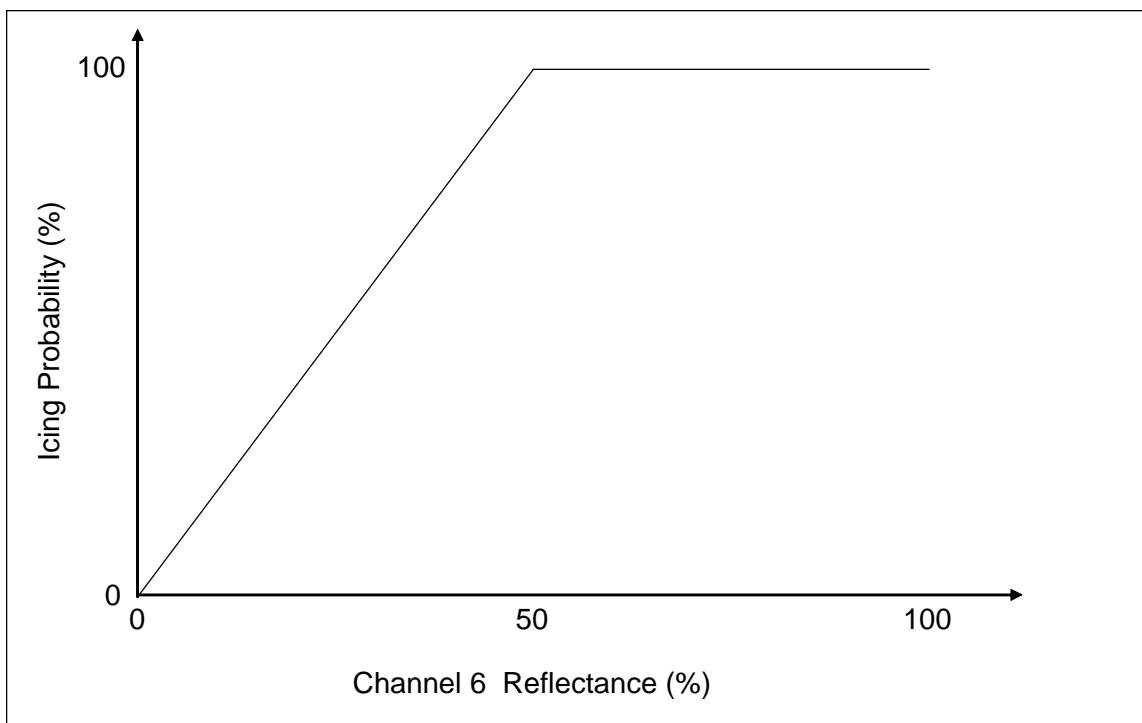


Figure 9. P06 Icing potential vs. channel 6 reflectance percentage (from Alexander 2005)



**c. P07 Reflectance Test**

The P07 test uses MODIS channel 7 ( $2.1 \mu m$ ), and is similar to the P06 test. Like the  $1.6 \mu m$  wavelength the  $2.1 \mu m$  wavelength has nearly identical real indexes of refraction for water and ice clouds, but different imaginary indexes of refraction. In this case the difference in the imaginary index of refraction is less than the P06 test. This fact makes it a little more difficult to distinguishing ice from water with the P07 test. The specifics of the test are depicted in Figure 10.

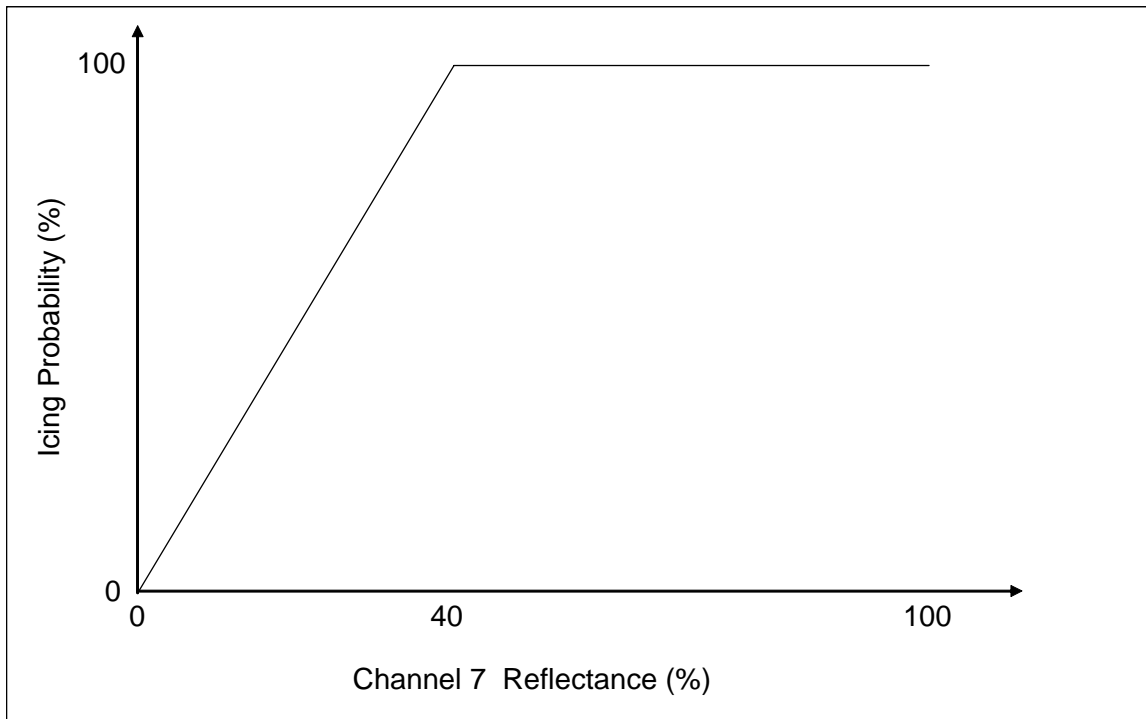


Figure 10. P07 icing potential vs. channel 7 reflectance percentage (from Alexander 2005)

**d. P22 Reflectance Test**

The P22 reflectance test uses MODIS channel 22 ( $3.9 \mu m$ ). This channel lies in the crossover region between incoming solar and outgoing terrestrial radiation making it difficult to distinguish the source of the sensed energy. Therefore, the emitted energy of the cloud must be subtracted from the total sensed value of the satellite to determine the total reflected solar energy. The total solar value can then be used to determine the phase of the cloud since

water clouds again reflect more energy than ice clouds. The threshold for water clouds, and therefore maximum icing potential was found to be  $>0.06$  which is where Alexander starts a rapid decrease in icing potential as depicted in Figure 11.

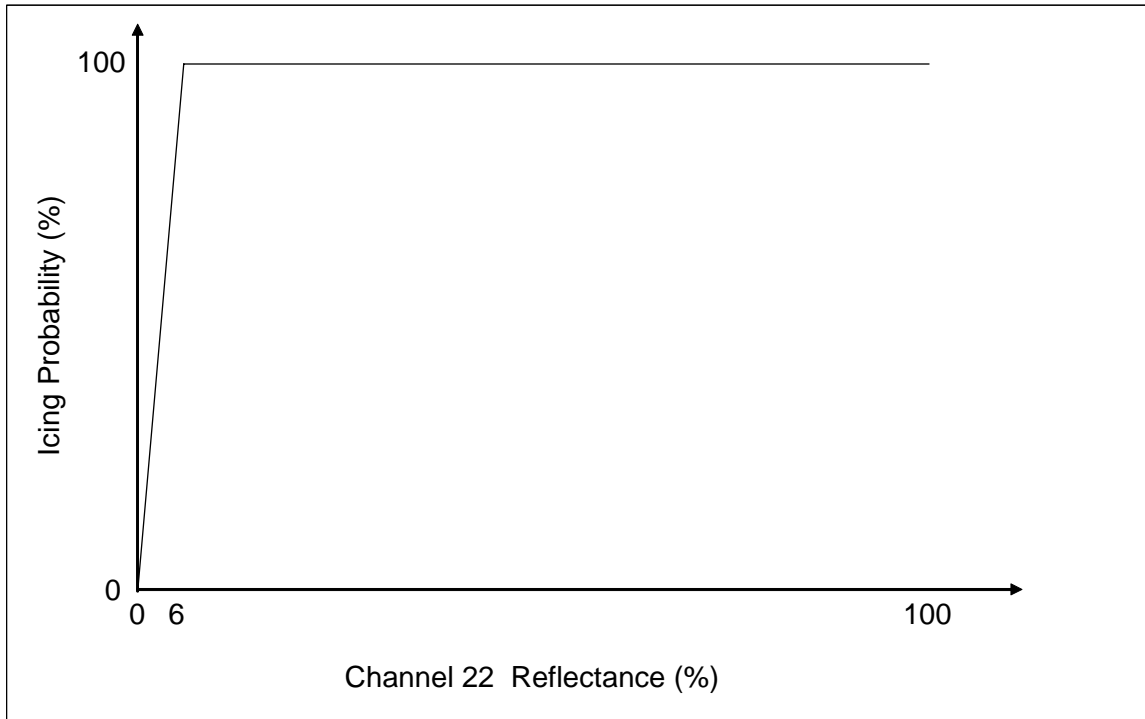


Figure 11. P22 icing potential vs. channel 22 reflectance percentage (from Alexander 2005).

**e. P26 Reflectance Test**

The P26 reflectance test uses MODIS channel 26 ( $1.38 \mu m$ ). This test is unique in that it is not attempting to determine where icing potential is high, but where there is no icing potential. This wavelength is highly susceptible to absorption by water vapor in the atmosphere which limits the energy seen by the satellite to that reflected by clouds so high in the atmosphere that they are almost certainly ice clouds. At these altitudes the temperature is too cold for the presence of SLW in any sensed clouds and therefore icing potential is negligible. The specifics of this test are depicted in Figure 12.

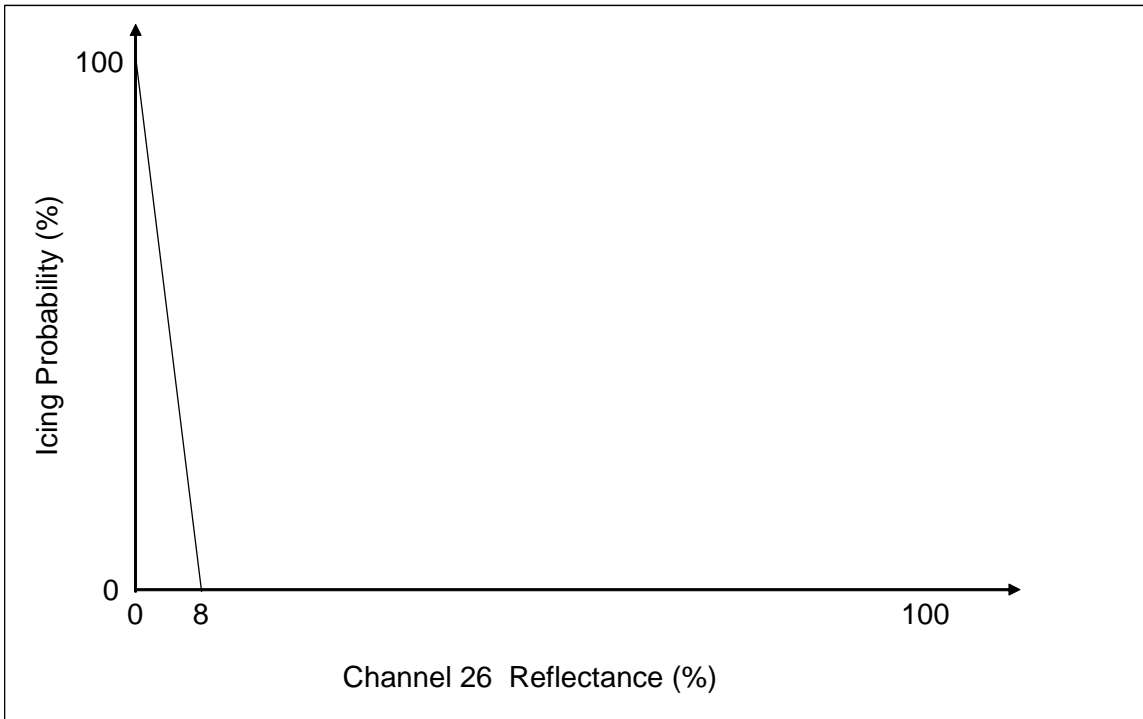


Figure 12. P26 icing potential vs. channel 26 reflectance percentage (from Alexander 2005)

## 2. Group II Reflectance Ratio Tests: P61 and P71

Ratio tests provide a more detailed determination of cloud phase than reflectance tests alone. Two tests are performed in this group using the previously discussed channel 1, 6, and 7 reflectance values. Reflectance values for channel one will be highest, and water clouds will have a higher reflectance than ice clouds in both channels 6 and 7. This means a high value from the ratio of channel 6 to channel 1 (P61) and channel 7 to channel 1 (P71) will indicate a high probability of water clouds. Since SLW produces airframe icing, high values of either ratio would indicate high icing potential. That said, there are situations where the ratio can be greater than 1, but they do not occur in clouds. Therefore, values greater than one were excluded from the icing potential test, and areas with values between 0 and 1 were included. P61 icing potential vs. ratio value is depicted in Figure 13. P71 icing potential vs. ratio value is depicted in Figure 14.

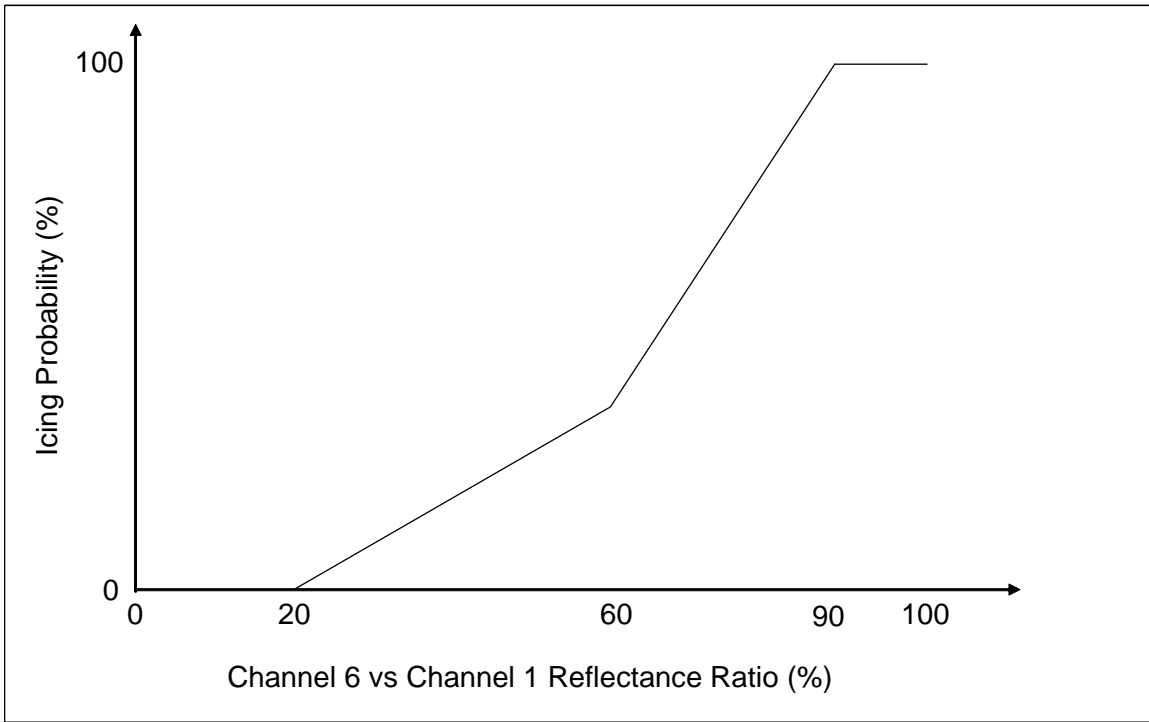


Figure 13. P61 Icing potential vs. P61 ratio (from Alexander 2005).

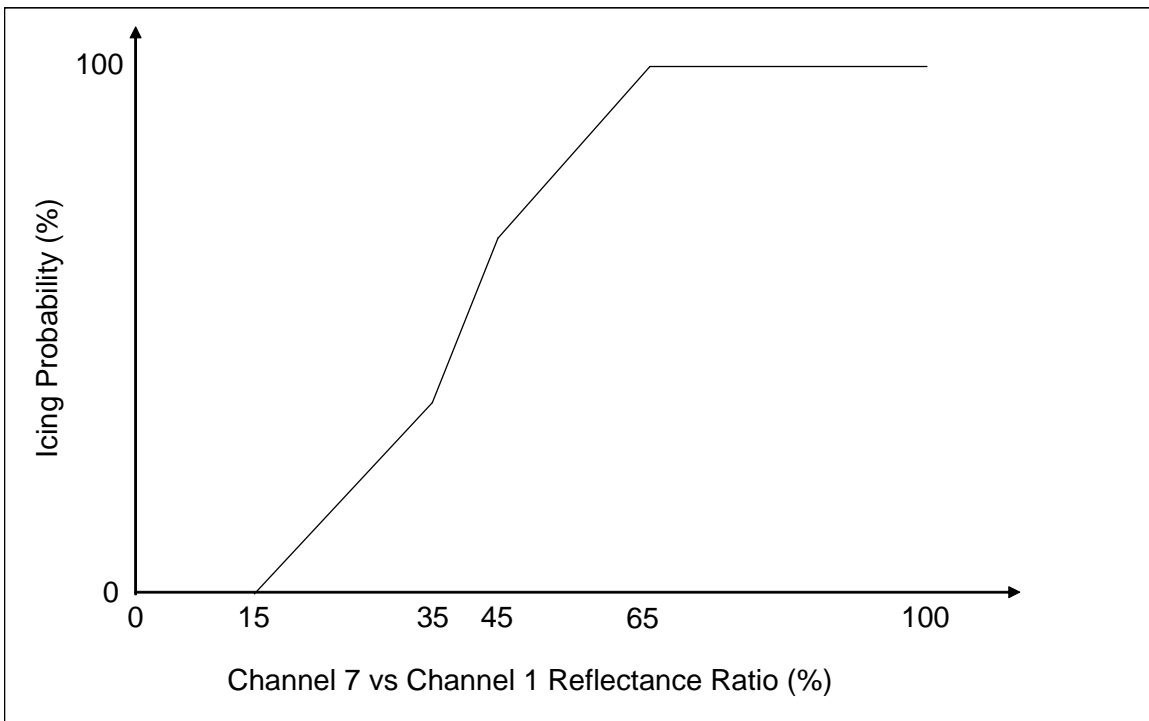


Figure 14. P71 Icing potential vs. P71 ratio (from Alexander 2005)

### 3. Group III Brightness Temperature Test (P31)

The P31 brightness temperature (BT) test uses MODIS channel 31 ( $11\ \mu\text{m}$ ). At this wavelength clouds are both good absorbers and good emitters. This is also the wavelength at which the earth's blackbody emission peaks. This means energy emitted by the earth is absorbed by the cloud and the cloud then reemits energy based on its temperature. Therefore the radiance detected by the satellite can be converted to cloud top temperature. Since the radiance detected only comes from the top few meters of the cloud the temperature within the cloud can not be directly measured, but if cloud tops are between 0 and  $-25^\circ\text{C}$  a large icing potential can be inferred. Figure 15 depicts the icing probability values used in Alexander (2005).

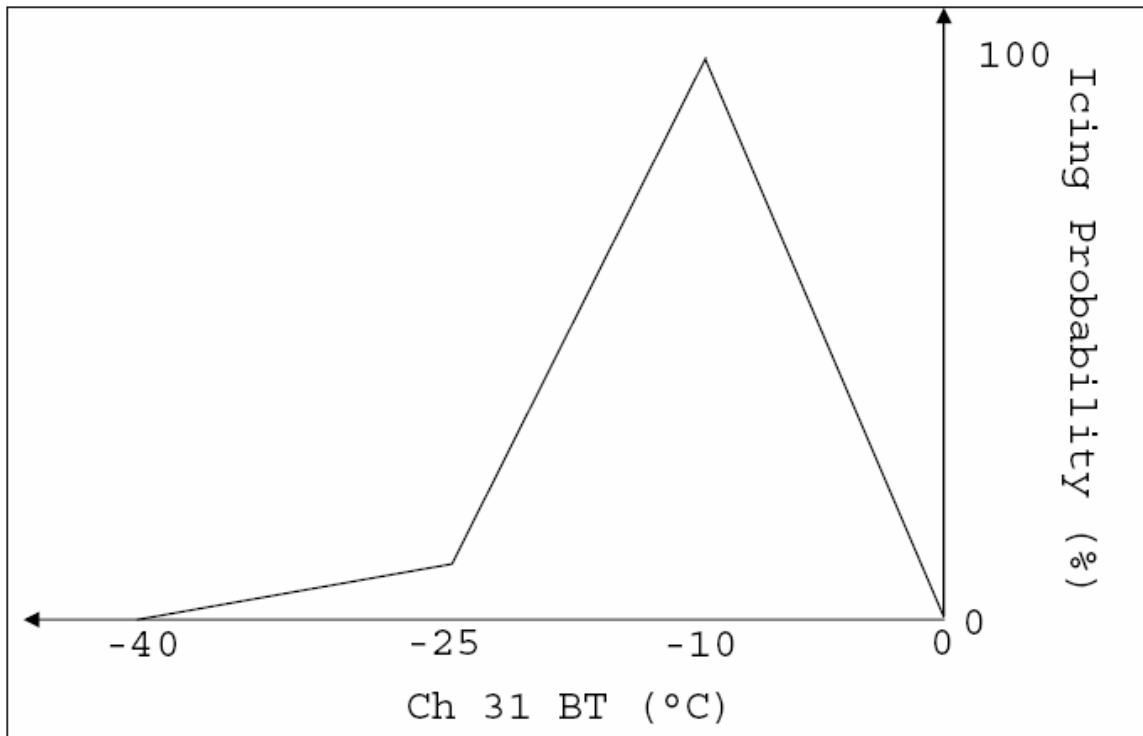


Figure 15. P31 Brightness Temperature probability values (from Alexander 2005)

### 4. Group IV Brightness Temperature Difference Tests

The brightness difference tests again allow for more accurate phase discrimination within the clouds. All tests in this group are designed to exploit the change in the imaginary index of refraction for water and ice clouds from one

wavelength to the next. Since the absorption coefficient is directly proportional to the imaginary index of refraction, and good absorbers are good emitters at a given wavelength, sensed brightness temperatures will vary for water and ice clouds as wavelength changes. This variation in sensed brightness temperature makes phase determination possible.

**a. BTD1 Brightness Temperature Difference Test**

The BTD1 test measures the difference between MODIS channels 22 ( $3.9 \mu m$ ) and 31 ( $11 \mu m$ ). During daylight hours energy is both reflected and emitted by clouds at the channel 22 wavelength. This causes channel 22 brightness temperatures to be greater than channel 31 brightness temperatures. Since water clouds reflect better at the channel 22 wavelength, water clouds have higher brightness temperatures than ice clouds. This leads to a greater difference between channel 22 and channel 31 temperatures in clouds where icing potential is high. The specifics of this test are found in Figure 16.

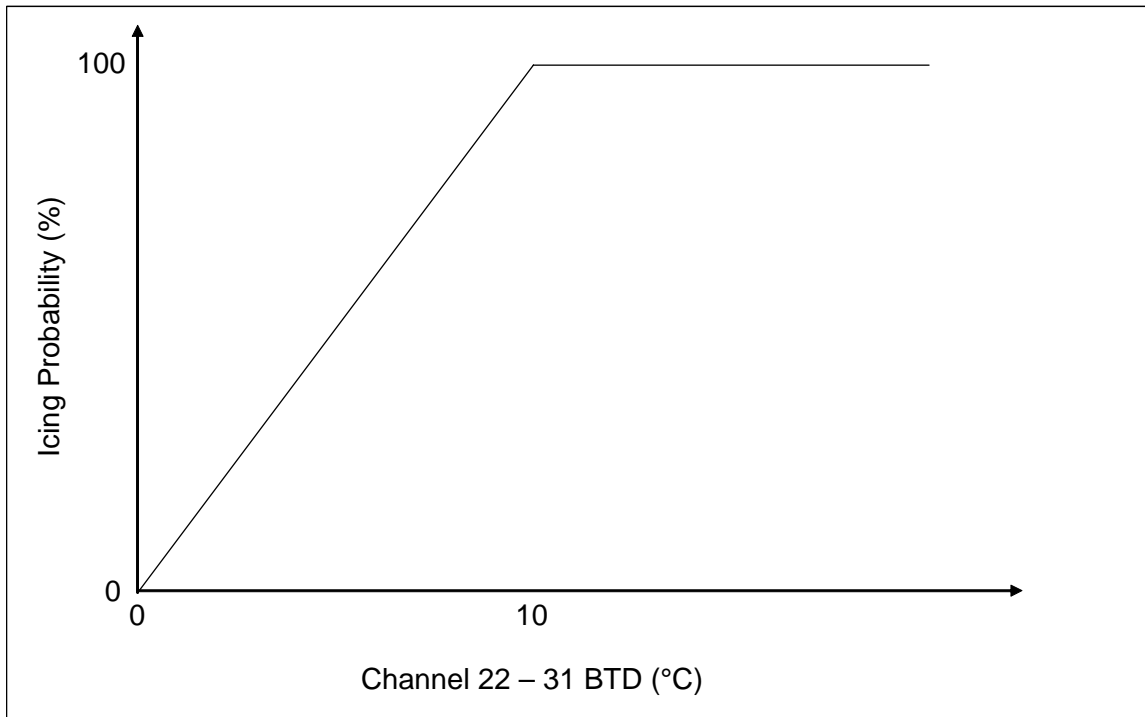


Figure 16. BTD1 icing potential vs Channel 22-31 brightness temperature difference (from Alexander 2005)

**b. BT D2 Brightness Temperature Difference Test**

The BT D2 test measures the difference between MODIS channels 29 ( $8.5 \mu\text{m}$ ) and 31 ( $11 \mu\text{m}$ ) brightness temperatures. At the channel 29 wavelength the absorption coefficient for both ice and water clouds are approximately the same. As you move toward the channel 31 wavelength the absorption coefficient increases for both water and ice clouds, but the ice absorption coefficient increases more than the water absorption coefficient. Since a good absorber is also a good emitter the channel 31 brightness temperatures for ice clouds will be lower than water clouds leading to a negative difference in water clouds, and positive in ice clouds. The specifics of the test are found in Figure 17.

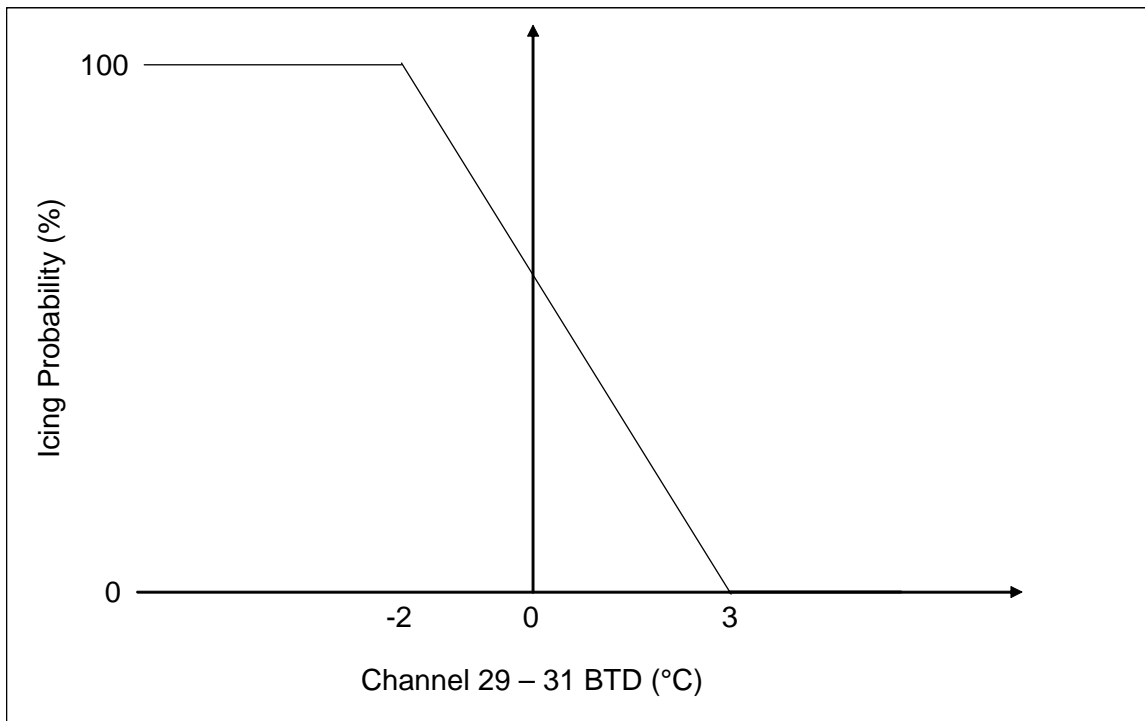


Figure 17. BT D2 icing potential vs. channel 29-32 brightness temperature difference (from Alexander 2005)

**c. BT D3 Brightness Temperature Difference Test**

The BT D3 test measures the difference between MODIS channels 31 ( $11 \mu\text{m}$ ) and 32 ( $12 \mu\text{m}$ ) brightness temperatures. This test attempts to help distinguish ice clouds from water clouds, but is limited in its ability to do so. The

absorption coefficients for both ice and water clouds increase between  $11 \mu m$  and  $12 \mu m$ . This means clouds are better absorbers, and therefore better emitters at the  $12 \mu m$  wavelength, which leads to slightly lower  $12 \mu m$  BTs. The result is that this difference is generally positive, but research by Inoue (1987) and Wieman (1990) found that cirrus clouds have a difference greater than 0.81 degrees, and thin cirrus have a difference greater than 1.51 degrees. This makes the test helpful in distinguishing cirrus clouds. The specifics of the test are found in Figure 18.

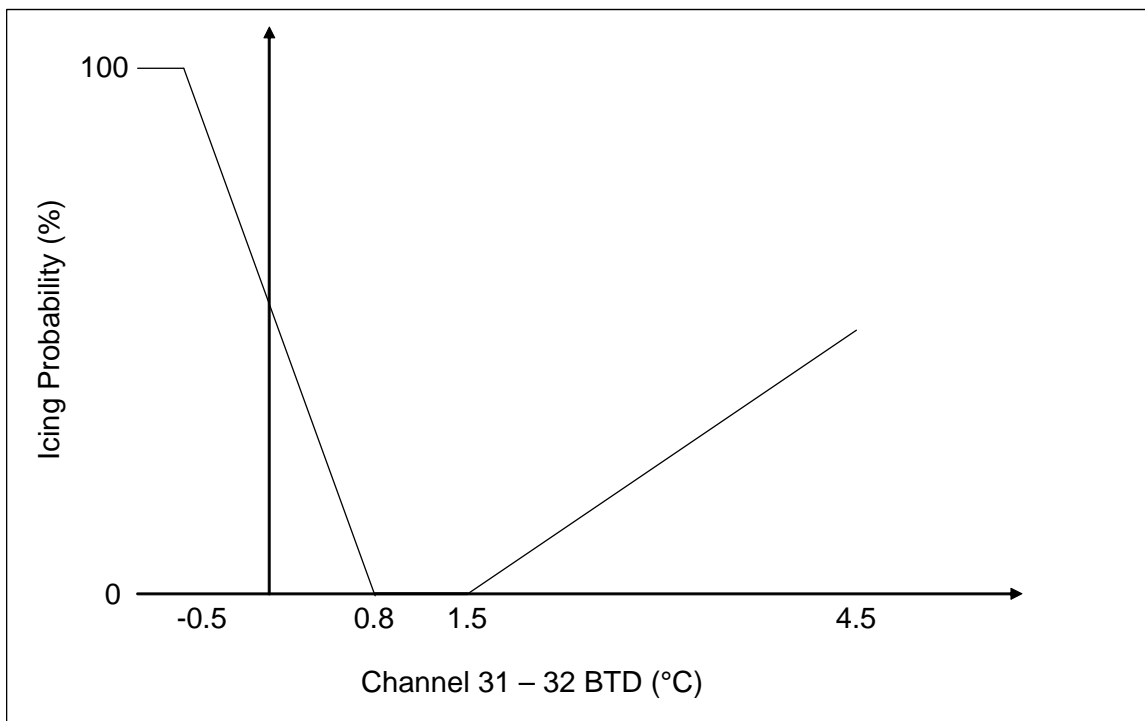


Figure 18. BT D3 icing potential vs. channel 31-32 brightness temperature difference (from Alexander 2005)

**d. BT D4 Trispectral Brightness Temperature Difference Test**

This test is equal to the BT D2 value minus BT D3 value, and is based on research done by Strabala et al. (1994). The absorption coefficient for water clouds increase more between  $11 \mu m$  and  $12 \mu m$  than between  $8.5 \mu m$  and  $11 \mu m$  which makes the BT D3 value for water clouds larger than the BT D2 values, and the opposite is true for ice. Since the BT D2 values for water clouds



are negative and the BTD3 values for water clouds are positive then the difference for water clouds will be negative. As stated earlier the opposite is true for ice clouds whose difference will be positive. If the cloud contains both water and ice, the value will be close to zero. The specifics of the test are shown in Figure 19.

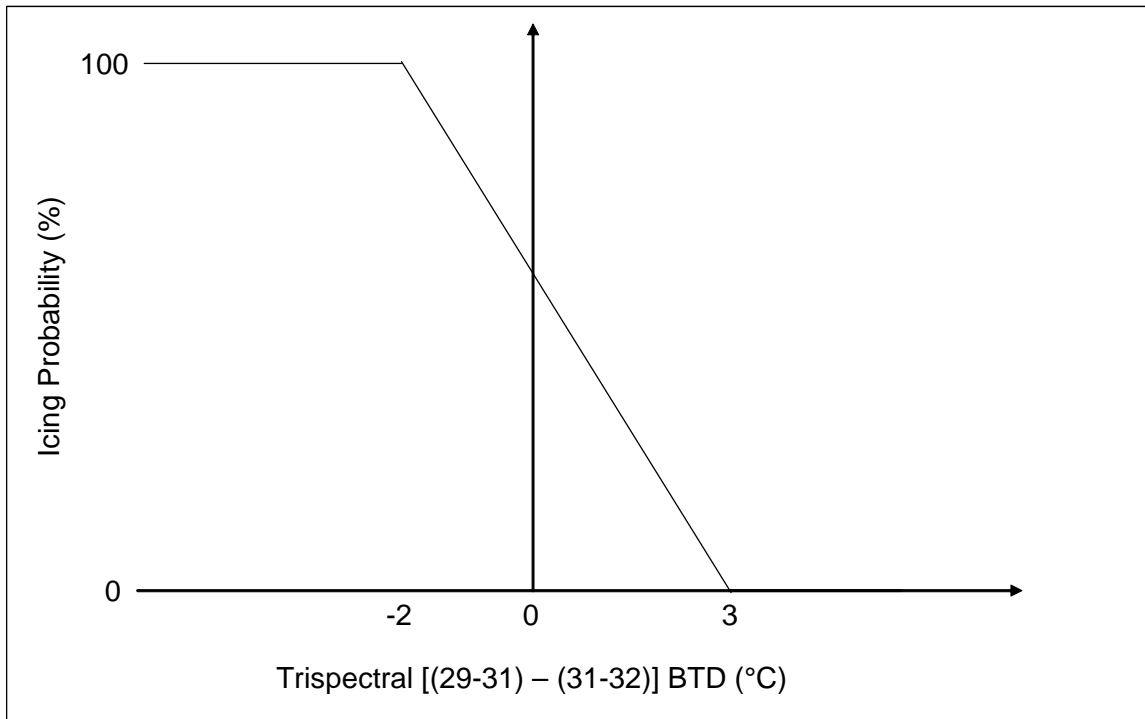


Figure 19. BTD4 icing potential vs. trispectral brightness temperature difference (from Alexander 2005)

### 5. The Final MODIS Algorithm Test

To calculate the final icing potential value Alexander (2005) examined all of the tests within a group and took the highest icing potential value found for each pixel to create the final group icing potential field. This moved the bias toward high icing potential. Once all of the final group fields were created, the final group values for each pixel location were multiplied together and the fourth root taken to determine the pixel value in the final icing potential field. This process is displayed in Figure 20.

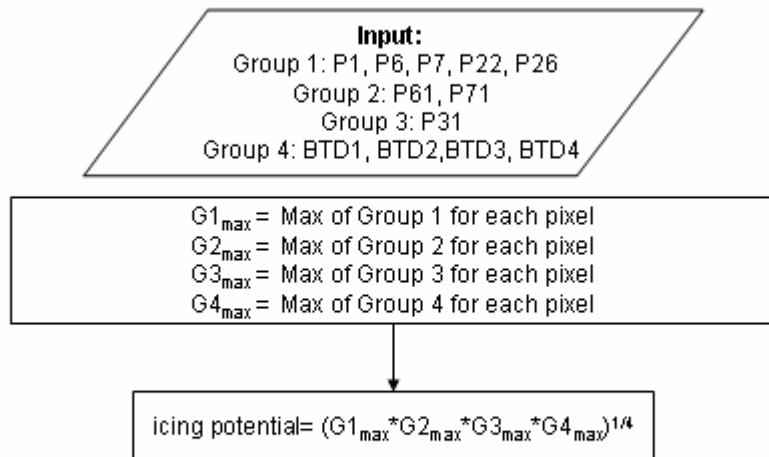


Figure 20. Illustration of the final aircraft icing potential test (Alexander 2005).

Table 2. Channel specifications for the MODIS platform (after MODIS web 2006)

Primary Use	Band	Bandwidth <sup>1</sup>	Spectral Radiance <sup>2</sup>	Required SNR <sup>3</sup>
Land/Cloud/Aerosols Boundaries	1	620 - 670	21.8	128
	2	841 - 876	24.7	201
Land/Cloud/Aerosols Properties	3	459 - 479	35.3	243
	4	545 - 565	29.0	228
	5	1230 - 1250	5.4	74
	6	1628 - 1652	7.3	275
	7	2105 - 2155	1.0	110
Ocean Color/ Phytoplankton/ Biogeochemistry	8	405 - 420	44.9	880
	9	438 - 448	41.9	838
	10	483 - 493	32.1	802
	11	526 - 536	27.9	754
	12	546 - 556	21.0	750
	13	662 - 672	9.5	910
	14	673 - 683	8.7	1087
	15	743 - 753	10.2	586
Atmospheric Water Vapor	16	862 - 877	6.2	516
	17	890 - 920	10.0	167
	18	931 - 941	3.6	57
	19	915 - 965	15.0	250
Primary Use	Band	Bandwidth <sup>1</sup>	Spectral Radiance <sup>2</sup>	Required NE[delta]T(K) <sup>4</sup>
Surface/Cloud Temperature	20	3.660 - 3.840	0.45(300K)	0.05
	21	3.929 - 3.989	2.38(335K)	2.00
	22	3.929 - 3.989	0.67(300K)	0.07
	23	4.020 - 4.080	0.79(300K)	0.07
Atmospheric Temperature	24	4.433 - 4.498	0.17(250K)	0.25
	25	4.482 - 4.549	0.59(275K)	0.25
Cirrus Clouds Water Vapor	26	1.360 - 1.390	6.00	150(SNR)
	27	6.535 - 6.895	1.16(240K)	0.25
	28	7.175 - 7.475	2.18(250K)	0.25
Cloud Properties	29	8.400 - 8.700	9.58(300K)	0.05
Ozone	30	9.580 - 9.880	3.69(250K)	0.25
Surface/Cloud Temperature	31	10.780 - 11.280	9.55(300K)	0.05
	32	11.770 - 12.270	8.94(300K)	0.05
Cloud Top Altitude	33	13.185 - 13.485	4.52(260K)	0.25
	34	13.485 - 13.785	3.76(250K)	0.25
	35	13.785 - 14.085	3.11(240K)	0.25
	36	14.085 - 14.385	2.08(220K)	0.35

<sup>1</sup> Bands 1 to 19 are in nm; Bands 20 to 36 are in  $\mu\text{m}$

<sup>2</sup> Spectral Radiance values are ( $\text{W}/\text{m}^2 \cdot \mu\text{m}\cdot\text{sr}$ )

<sup>3</sup> SNR = Signal-to-noise ratio

<sup>4</sup> NE(delta)T = Noise-equivalent temperature difference

Note: Performance goal is 30-40% better than required

### III. PROCEDURE

The synoptic situation was closely monitored in early 2006 to determine when subtropical systems would be transiting the northeastern United States and southeastern Canada. MODIS imagery and PIREP data was subsequently collected for January 15, 18, 23, and 25, 2006 over the same area examined by Alexander in 2005. Although using the same area was not necessary, it was a logical choice since air traffic is much denser in the northeastern United States than elsewhere in the country. MODIS imagery files were collected from the National Aeronautics and Space Administration's (NASA) website at [http://daac.gsfc.nasa.gov/daac-bin/MODIS/Data\\_order.pl](http://daac.gsfc.nasa.gov/daac-bin/MODIS/Data_order.pl). PIREP data was collected from the National Oceanic and Atmospheric Administration's (NOAA) Aviation Digital Data Service (ADDS) website at <http://adds.aviationweather.gov/pireps/>.

#### A. RAW MODIS FILE INVESTIGATION

MODIS imagery was analyzed using Alexander's algorithm, and the procedures outlined in Alexander (2005). The raw files were processed using MATLAB program files originally created by Dr. Shaima Nasiri, adapted by Alexander (2005), and further adapted to process the new MODIS files. While the program files were adapted, the MODIS based aircraft icing potential algorithm was not changed. MODIS Icing potential fields were then compared to the 133 total (109 positive, 24 negative) PIREPS collected within three hours of the MODIS image times. All pixels within 25 miles of each PIREP were examined to determine the mean and median value of icing potential in that area. The maximum value of either the mean or median was used to determine the MODIS icing potential ( $MODIS_{pot}$ )

#### B. MM5 MODEL DATA INVESTIGATION

Air Force Weather Agency (AFWA) MM5 Model Data was investigated using the GARP program. More specifically GARP's model sounding capability was utilized to determine the temperature (T) and dew point temperature ( $T_d$ ) at each PIREP location and flight level. If the PIREP fell within one hour of a

forecast period (ie. 1400-1600 for the 1500Z forecast time) that forecast period's values were used in calculations. If the PIREP fell in the middle hour between forecasts (1600-1700 given the standard forecast times of 1500 and 1800) the values for both the early and late forecast were collected. An example of model sounding output is shown in Figure 21.

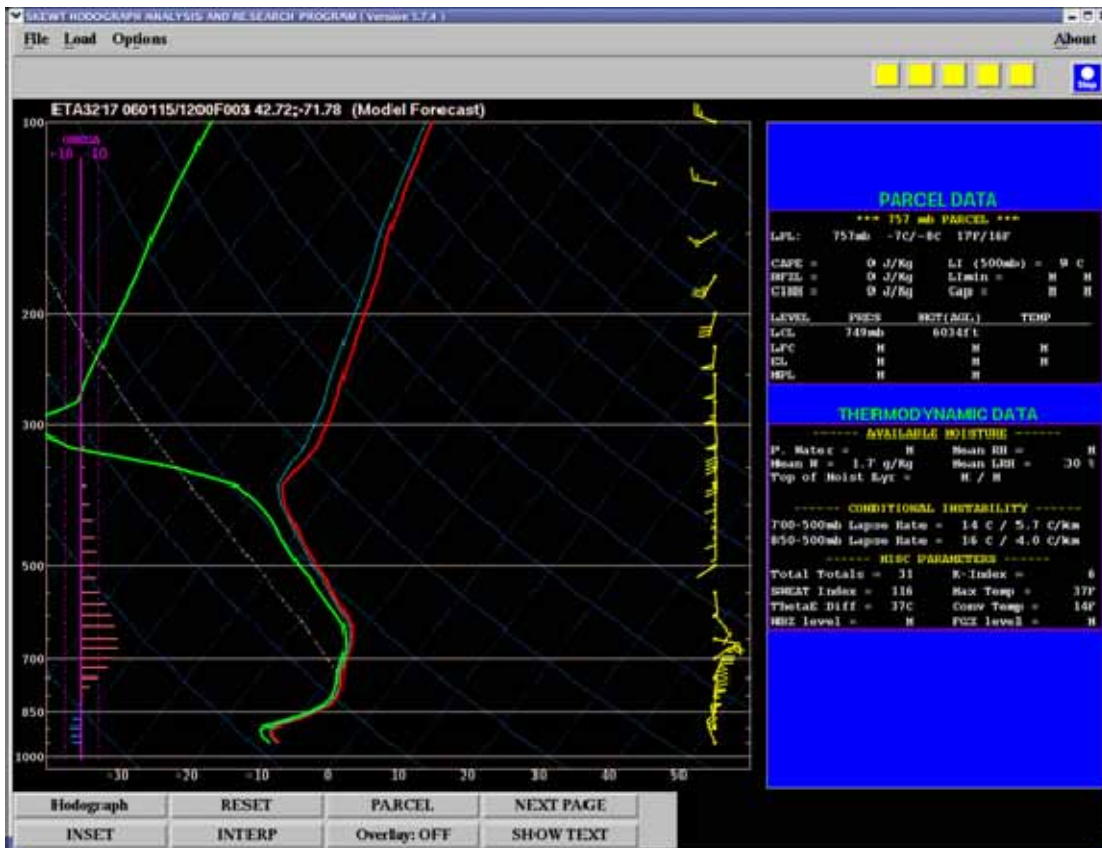


Figure 21. Sample GARP model sounding output

The procedure for collecting the model data was straight forward. The GARP interface allows for the input of an exact latitude and longitude pair so a sounding could be created at each PIREP location. Once a sounding was created, the pressure level associated with the flight level reported in the PIREP was determined by placing the cursor within the field and reading the altitude and pressure level of the cursor. After the pressure level of the PIREP was determined, it was manually input using the PARCEL menu button depicted in Figure 21. The parcel's data, including T and  $T_d$ , was then displayed in the upper

right portion of the screen. The T and T<sub>d</sub> values were then recorded in an Excel spreadsheet for future use in calculations. This process was repeated for all 133 PIREPS, and twice for each PIREP if it fell in a middle hour between forecasts.

## **C. TOTAL ICING POTENTIAL CALCULATIONS**

### **1. Model Icing Potential Assignment**

The first calculation required before assigning an icing potential value is determining the relative humidity (RH) at the PIREP location and altitude. This was accomplished using a simple equation used by the National Weather Service (NWS), and is listed in Table 3. The equation approximates RH within 0.6% from -25 through 45 degrees Celsius. While icing can be encountered below -25 degrees Celsius, the icing potential at these temperatures is very low.

#### ***a. RH Icing Potential Assignment***

Icing potential values were assigned to the RH values at each PIREP location using an RHmap similar to the CIP in Bernstein et al. (2005). The actual RHmap used here is slightly more simple than the operational CIP RHmap, in that it has fewer turning points. For the purpose of calculations, the RHmaps are essentially the same. The exact RHmap used here is shown in Figure 5.

#### ***b. T Icing Potential Assignment***

Icing potential values were assigned to the T values collected at each PIREP location using 2 separate Tmaps. The first Tmap is based on research conducted by Sand et al. in (1984) and is identical to the MODIS Channel 31 brightness temperature test used in the MODIS algorithm. The second Tmap is from the CIP as described in Bernstein et al. 2005. Like the CIP based RHmap, the actual CIP based Tmap used here is slightly modified, but effectively the same. Both Tmaps used here are displayed in Figure 6.

### **2. Eight Test Calculations**

Eight test calculations were made using both the Alexander based Tmap and the CIP based Tmap. The calculations were designed to accomplish several things. First, was to determine which Tmap would yield the best results. Second, to determine which method of determining T and T<sub>d</sub> between forecast

hours would yield the best results, and third, to determine the best weighting of model parameters in the icing potential calculations.

**a. MM5\_1**

The MM5\_1 Icing potential calculation uses the model T and T<sub>d</sub> values from the forecast hours +/- 1hr, and averages the values in the middle hour between forecasts. The RH values in the middle hour are calculated using the averaged T and T<sub>d</sub> values. The T, T<sub>d</sub> and RH values calculated in this manner have the subscript 1, and the icing potential values assigned from the Tmap and RHmap have the subscript 1pot. The actual equation used can be found in Table 3. This test gives equal weight to both T and RH icing potential values when calculating the model portion of the icing potential calculation, and also weighs the total model and MODIS portion equally. This test, as with 7 out of the 8 calculations, uses roots in the calculations. Since all icing potential values are between 0 and 1 multiplying them together, and taking root also produces a value between 0 and 1. For example:  $\sqrt{.89 \times .95} = .9195$ .

**b. MM5\_2**

The MM5\_2 Icing potential calculation uses the model T and T<sub>d</sub> values from the forecast hours +/- 1.5hrs. The RH values are simple calculations using these values. The T, T<sub>d</sub> and RH values calculated in this manner have the subscript 2, and the icing potential values assigned from the Tmap and RHmap have the subscript 2pot. The actual equation used can be found in Table 3. Apart from the method for determining the T and RH, the MM5\_2 calculation is the same as the MM5\_1.

**c. MM5\_1\_1**

The MM5\_1\_1 icing potential calculation uses the subscript 1pot model icing potential values found in the MM5\_1 calculation. The difference between the MM5\_1 and MM5\_1\_1 test is the weighting of the T derived icing potential value in the model portion of the total icing potential. In this case the T potential is multiplied by itself and the RH potential, and the cube root is taken to determine the total model potential. This effectively makes the model T value

more dominant in the icing potential calculation compared to RH. The actual equation used can be found in Table 3.

Table 3. Model icing potential calculations [table titles go at the top]

Variable	Formula
Relative Humidity (RH)	$RH \approx 100 \left( \frac{112 - 0.1T + T_d}{112 + 0.9T} \right)^8$ (National Weather Service 2005)
Icing potential using average T and Td in the middle hour (RH calc. with same) (MM5_1)	$MM5\_1 = \sqrt{(\sqrt{T_{1pot}} \times RH_{1pot}) \times MODIS_{pot}}$
Icing potential using forecast T and Td +/- 1.5 hrs (RH calc. with same)(MM5_2)	$MM5\_2 = \sqrt{(\sqrt{T_{2pot}} \times RH_{2pot}) \times MODIS_{pot}}$
Icing potential test 1 using T <sub>1pot</sub> and RH <sub>1pot</sub> (MM5_1_1)	$MM5\_1\_1 = \sqrt{(\sqrt[3]{T_{1pot} \times T_{1pot} \times RH_{1pot}}) \times MODIS_{pot}}$
Icing potential test 1 using T <sub>2pot</sub> and RH <sub>2pot</sub> (MM5_2_1)	$MM5\_2\_1 = \sqrt{(\sqrt[3]{T_{2pot} \times T_{2pot} \times RH_{2pot}}) \times MODIS_{pot}}$
Icing potential test 2 using T <sub>1pot</sub> and RH <sub>1pot</sub> (MM5_1_2)	$MM5\_1\_2 = \sqrt{(\sqrt[3]{T_{1pot} \times RH_{1pot} \times RH_{1pot}}) \times MODIS_{pot}}$
Icing potential test 2 using T <sub>2pot</sub> and RH <sub>2pot</sub> (MM5_2_2)	$MM5\_2\_2 = \sqrt{(\sqrt[3]{T_{2pot} \times RH_{2pot} \times RH_{2pot}}) \times MODIS_{pot}}$
Icing potential test 3 (MM5_3)	$MM5\_3 = 0.6 \times MODIS_{pot} + 0.2 \times MM5\_1\_2_{model\_pot} + 0.2 \times MM5\_2\_2_{model\_pot}$
Icing potential test 4 (MM5_4)	$MM5\_4 = \sqrt{\left( \frac{MM5\_1\_2_{model\_pot} + MM5\_2\_2_{model\_pot}}{2} \right) \times MODIS_{pot}}$



**d. MM5\_2\_1**

The MM5\_2\_1 icing potential calculation uses the subscript 2pot model icing potential values found in the MM5\_2 calculation. Otherwise, it is calculated in the same manner as the MM5\_1\_1 calculation. The actual equation used can be found in Table 3.

**e. MM5\_1\_2**

The MM5\_1\_2 icing potential calculation again uses the subscript 1pot model icing potential values, and is very similar to the MM5\_1\_1 test. The only difference is that the RH potential value is multiplied twice instead of the T potential value. Again, this effectively makes the RH potential more dominant in the icing potential calculation compared to T. The actual equation used can be found in Table 3.

**f. MM5\_2\_2**

The MM5\_2\_2 icing potential calculation uses the subscript 2pot model icing potential values, but is otherwise the same as the MM5\_1\_2. The actual equation used can be found in Table 3.

**g. MM5\_3**

The MM5\_3 icing potential calculation was added after early calculations revealed that the MM5\_1\_2 and MM5\_2\_2 seemed to produce favorable results. For that reason, the model icing potential values for those two tests were used in this calculation, which is the only calculation that does not use roots. It simply takes a percentage of the MODIS icing potential value, the model portion of the MM5\_1\_2 icing potential value, and the model portion of the MM5\_2\_2 icing potential value. Clearly, there are infinite weighting possibilities to this calculation, but the equation found in table 3 is the only variation used here. 60% of the MODIS icing potential value was added to 20% of both the MM5\_1\_2 and \_2\_2 model icing potential values. Since all values in the calculation must be between 0 and 1, the calculated potential will also be between 0 and 1. The actual equation used can be found in Table 3.

***h. MM5\_4***

The MM5\_4 icing potential calculation was also added after early calculations revealed that the MM5\_1\_2 and MM5\_2\_2 seemed to produce favorable results. In this calculation, the model portion of the total icing potential in MM5\_4 is simply an average of the model portion of the MM5\_1\_2 and MM5\_2\_2 icing calculations. This average is then multiplied by the MODIS potential value, and the root is taken. The actual equation used can be found in Table 3.

**D. VERIFICATION**

A large portion of the evaluation was modeled after the verification used by Alexander (2005). This allowed for direct comparison with his results. For all calculations (16 total between the Alexander based Tmap and the CIP Tmap) and the MODIS icing potential, a value of 0.5 or greater at the PIREP locations was considered high icing potential. Less than 0.5 was considered a low icing potential. These potential values were then compared to the 109 positive icing PIREPs and 24 negative icing PIREPS to determine how many PIREPS were correctly detected.

After the comparisons were made, the probability of detection (POD) and probability of correct null (PODno) were calculated for all methods of icing potential prediction. POD is simply the number of correctly detected positive icing PIREPs divided by the total number of positive icing PIREPs. PODno is the number of correctly detected negative icing PIREPS divided by the total number of negative icing PIREPs. In the case of the MODIS icing potential the area efficiency at the .5 threshold was also calculated for comparison with Alexander's results. Area efficiency is the POD value divided by the total area of diagnosed icing.

The remainder of the verification was designed to determine which method of calculating model icing potential provided the most value to the total icing potential calculation. To accomplish this, the threshold for high icing potential was varied from 0 to 1 in increments of 0.1. At each increment the POD, PODno, and false alarm fraction (FAF) were calculated for the MODIS

potential and the 16 calculated total potentials for use in receiver operating characteristic (ROC) curves. The details of ROC curves will be explained in Chapter IV.

## **IV. RESULTS**

### **A. RAW MODIS FILE INVESTGATION RESULTS AND MODIS ICING POTENTIAL RESULTS**

The initial investigation of the raw MODIS data fields revealed that there was a significant noise problem visible on all days. The noise was not always visible in the same channels, but always in a field used in Alexander (2005) MODIS based algorithm. While Alexander (2005) limited his study to the use of MODIS files from the Terra platform, data from both the Terra and Aqua platforms were investigated here. The January 15, 2006 case was Terra based data, and the remainder of the cases (January 18, 23 and 25, 2006) were Aqua based.

After viewing the fields created by the MODIS algorithm tests, it became apparent that the Aqua based cases had a large amount of noise in the Channel 6 reflectance field. An example of this is found in Figure 22. Since this field is used in two of the twelve tests, it was very important to identify and account for the noise. An investigation of the raw data revealed that the noise had values well above 1. Since reflectance values must be between 0 and 1, the noise was easily filtered out using MATLAB to index the pixels with erroneous values. Once the noise pixels were indexed, the noise values were replaced with no value. This was done to maintain the shape and structure of the data field, which was very important for comparing PIREP locations with pixel locations. An example of the corrected field can be seen in Figure 23. The MODIS algorithm was then run using the filtered fields. After comparing the resultant MODIS icing potential field with PIREP locations, it was found that in no case were the pixels within 25 miles of a PIREP more than half noise. This finding allowed for a reasonably accurate determination of MODIS based icing potential at the PIREP location, but the validity of area efficiency calculations may be limited.

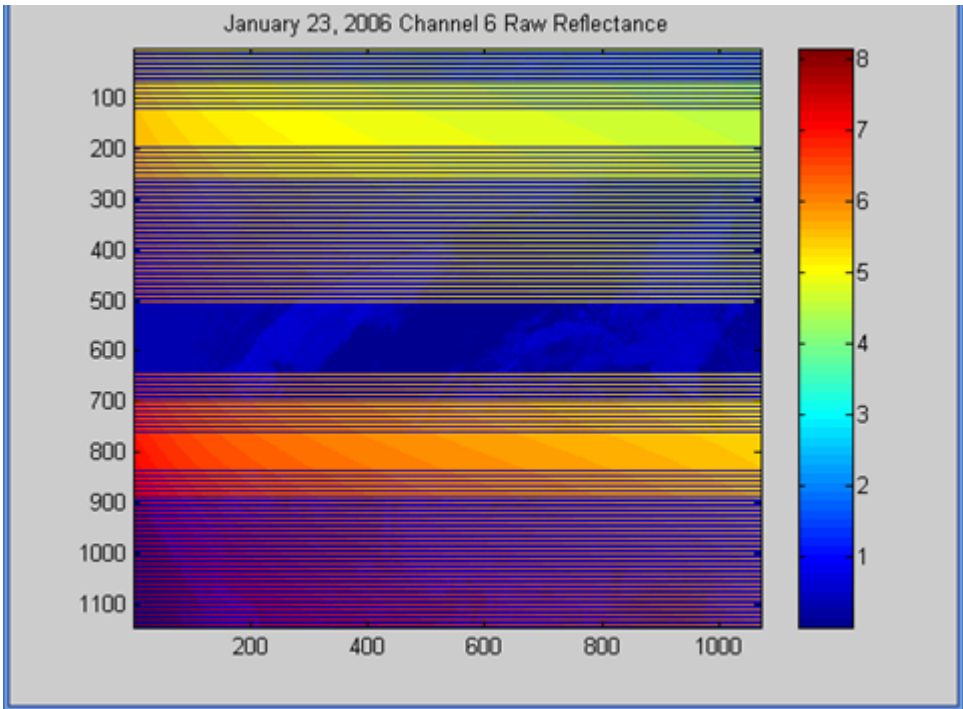


Figure 22. Raw January 23, 2006 channel 6 reflectance field

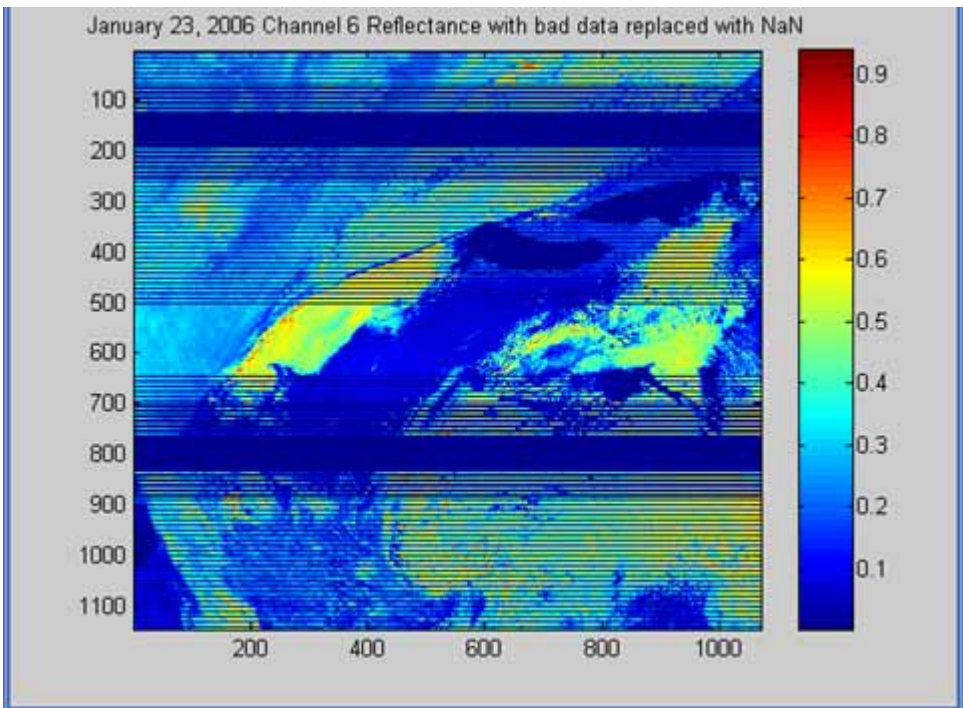


Figure 23. Filtered January 23, 2006 channel 6 reflectance field

The MODIS algorithm tests also revealed that the Terra based case also had a noise problem. The noise here was found in the channels 22 and 29 brightness temperature fields, and could not be filtered out. An example of this noise can be found in Figure 24. At first glance it may appear that there is not any noise, but a close inspection reveals noise in the blue-green shades in the upper middle portion of the field. An investigation of the raw data revealed that the noise was on the order of 3 Kelvin, but determining which pixels were noise against the valid data proved too difficult. This was a very significant finding considering the fact that a 3 Kelvin magnitude difference in the brightness temperature difference tests could significantly change the icing potential assigned to the pixel. Given the small area affected by the noise, it was decided that these fields would be used with the noise in place.

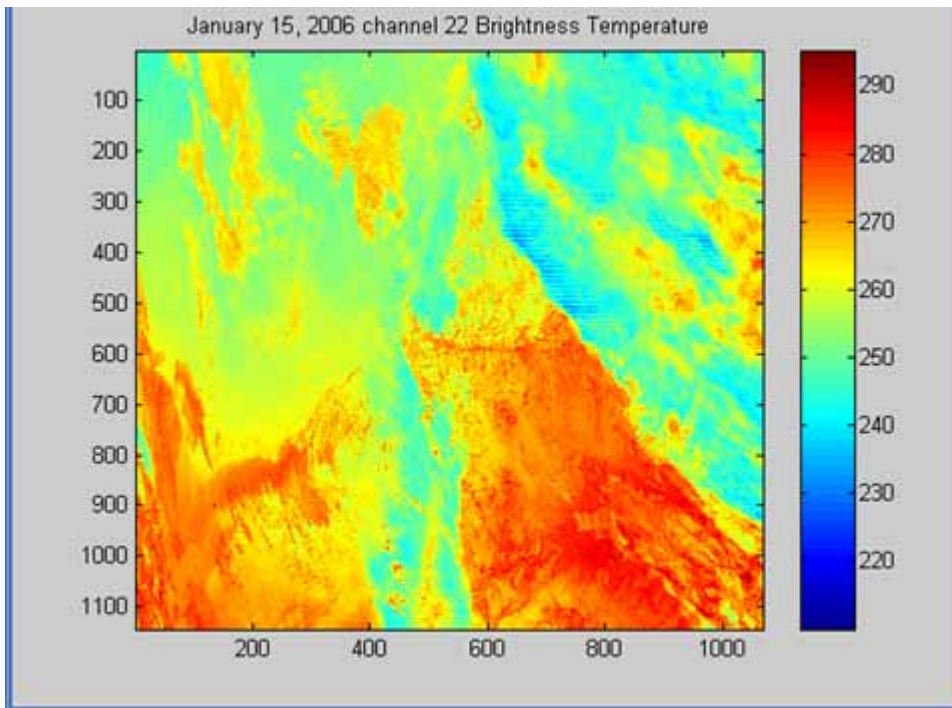


Figure 24. Channel 22 brightness temperature field from January, 15, 2006

The final results of the MODIS based icing potential algorithm compared to the 133 PIREPs within 3hrs of the 2006 MODIS valid times produced an overall POD of 72%, a PODno of 25%, with an average area efficiency of

$0.1902 \times 10^{-5} km^{-2}$ . These results compared favorably with Alexander (2005) findings based on 46 PIREPs within a 3hrs of the 2003 MODIS fields. His investigation produced a POD of 62.5%, a PODno of 33.3%, and an area efficiency of  $0.1409 km^{-2}$ .<sup>1</sup>

## **B. MODEL ICING POTENTIAL CALCULATION RESULTS**

The initial assessment of the value added by the various model icing potential calculations occurred at the 0.5 threshold using PIREPs within 3 hours of the MODIS valid times. This allowed for a comparison with the results already discussed.

The results using the Alexander Tmap values in calculations can be found in Table 4. Row 1 shows the results of the MODIS icing potential alone while the remainder of the rows show the results using the calculations described in chapter III. At first glance it might appear that the addition of the model data decreased the MODIS algorithm's ability to correctly assess icing potential since the POD value decreased in every case except one, the MM5\_3. However, one must look at the PODno values, which are at worst the same as the MODIS algorithm, and at best, are 100% greater. A close inspection reveals that the MM5\_1\_2, MM5\_2\_2, and the MM5\_4 icing potential calculations produce the best combination of POD and PODno values. The common thread between these three tests is that they all weight relative humidity more in the model portion of the total icing potential calculation. Also important to note, is that in every case except the MM5\_3, the decrease in POD was less than the increase in PODno.

One new variable appears in Table 4 that has not been previously discussed. FAF in column three is the false alarm fraction, and is simply  $1 - \text{PODno}$ . The calculation was necessary, since it is one of the plotted values in a ROC curves that will be discussed later.

---

<sup>1</sup> It is assumed that the area efficiency value found in Alexander 2005 is missing a  $\times 10^{-2}$ , but this can not be verified without repeating Alexander's study.

Table 4. Results using T icing potential values from the Alexander Tmap, and 3 Hour PIREPs

	POD	POD-NO	FAF	threshold	corr +	corr -
Modis	0.72	0.25	0.75	0.50	79.00	6.00
mm5_1	0.68	0.42	0.58	0.50	74.00	10.00
mm5_2	0.67	0.46	0.54	0.50	73.00	11.00
mm5_1_1	0.69	0.33	0.67	0.50	75.00	8.00
mm5_2_1	0.71	0.33	0.67	0.50	77.00	8.00
mm5_1_2	0.67	0.50	0.50	0.50	73.00	12.00
mm5_2_2	0.67	0.50	0.50	0.50	73.00	12.00
mm5_3	0.77	0.25	0.75	0.50	84.00	6.00
mm5_4	0.67	0.50	0.50	0.50	73.00	12.00

The results using the CIP Tmap values and calculations can be found in Table 5. As in Table 4, row 1 lists the MODIS icing potential results followed by the rest of the calculations. The addition of model data again appears to decrease the POD values in all tests except the MM5\_3 calculation, and the MM5\_1\_2, the MM5\_2\_2, and the MM5\_4 again appear to have the best combination of POD and PODno. The similarities end there. In this case, the only tests that produced a greater increase in PODno than decrease in POD were the MM5\_1\_2, the MM5\_2\_2, and the MM5\_4. In the calculations using the Alexander Tmap this occurred in every case except the MM5\_3.

Table 5. Results using T icing potential values from the CIP Tmap, and 3 hour PIREPs

	POD	POD-NO	FAF	threshold	corr +	corr -
modis	0.72	0.25	0.75	0.50	79.00	6.00
mm5_1	0.66	0.29	0.71	0.50	72.00	7.00
mm5_2	0.67	0.29	0.71	0.50	73.00	7.00
mm5_1_1	0.62	0.29	0.71	0.50	68.00	7.00
mm5_2_1	0.64	0.29	0.71	0.50	70.00	7.00
mm5_1_2	0.67	0.38	0.63	0.50	73.00	9.00
mm5_2_2	0.68	0.42	0.58	0.50	74.00	10.00
mm5_3	0.80	0.21	0.79	0.50	87.00	5.00
mm5_4	0.67	0.42	0.58	0.50	73.00	10.00

While enlightening, the snap shot view displayed in Tables 4 and 5 seemed insufficient to determine which calculation added the most value to the



MODIS based icing potential algorithm. To aid in this determination, the threshold for high icing potential was varied 0 to 1 in increments of 0.1, and the results plotted in ROC curves. It should be noted that ROC curves use the FAF as one of the plotted variables and there are some who believe that it is not appropriate to look at positive and negative PIREPs together. Brown et al. (1997) argues that positive and negative PIREPs do not truly represent icing in the atmosphere since pilots do not feel obligated to report negative icing conditions. This leads to PIREPs overestimating icing conditions, but in the cases examined here, the days and areas were chosen to effectively guarantee large areas of icing. This would ensure a large number of PIREPs. In the cases examined here the areas had well over 50% of the area forecast as high icing potential. This could indicate that in these cases, the 109 positive and 24 negative PIREPs were more representative of the actual icing situation than previous studies that looked at larger areas. The traditional AE calculation was not possible in this case since the single point model calculations did not provide an area of forecast high icing potential. ROC curves were the only method available to compare the model calculations directly.

### **1. ROC Curves**

ROC curves are a valuable tool used to evaluate the performance of test thresholds in predicting reality. They are extremely useful here since we are attempting to determine which test provides the most added value to the MODIS based icing algorithm at the 0.5 high Icing potential threshold. While the actual values calculated at the 0.5 threshold have already been discussed, ROC curves provide a visual and mathematical representation of each calculation's value.

Table 6. Important ROC variables. Plotted variables highlighted in light grey.

Actual Icing vs. Icing Potential Prediction		
	Positive Icing Pirep	Negative Icing PIREP
High Icing Potential	POD Or True Positive Fraction (TPF)	False Alarm Fraction (FAF) Or Probability of False Alarm (PFA)
Low Icing Potential	False Negative Fraction (FNF)	PODno Or True Negative Fraction (TNF)
	POD+FNF=1	FAF+PODno=1

The variables needed to plot a ROC curve are displayed in Table 6. The two plotted variables are POD vs FAF. The resultant ROC curves from the use of the Alexander Tmap and the MODIS based icing algorithm can be seen in Figure 25. This figure will be used to explain ROC curve characteristics. POD is located on the Y axis, and the Probability of False Alarm (PFA, otherwise known as FAF) is located on the X axis. A one to one line is plotted for reference (black dot-dash line in Figure 25). The test lines are plotted from the upper right to the bottom left as the threshold value varies from a minimum to a maximum. A perfect test would plot a line across the graph at  $y = 1$  and down at  $x = 0$ . In this case the area under the curve would be one. This result would indicate a POD of 1 and a FAF of 0 (a FAF of zero also indicates a PODno of 1) was achieved by the test at some threshold value. This is never achieved in reality. Instead the test that plots farthest to the top and left of the graph (furthest from the one to one line) is considered to perform the best.

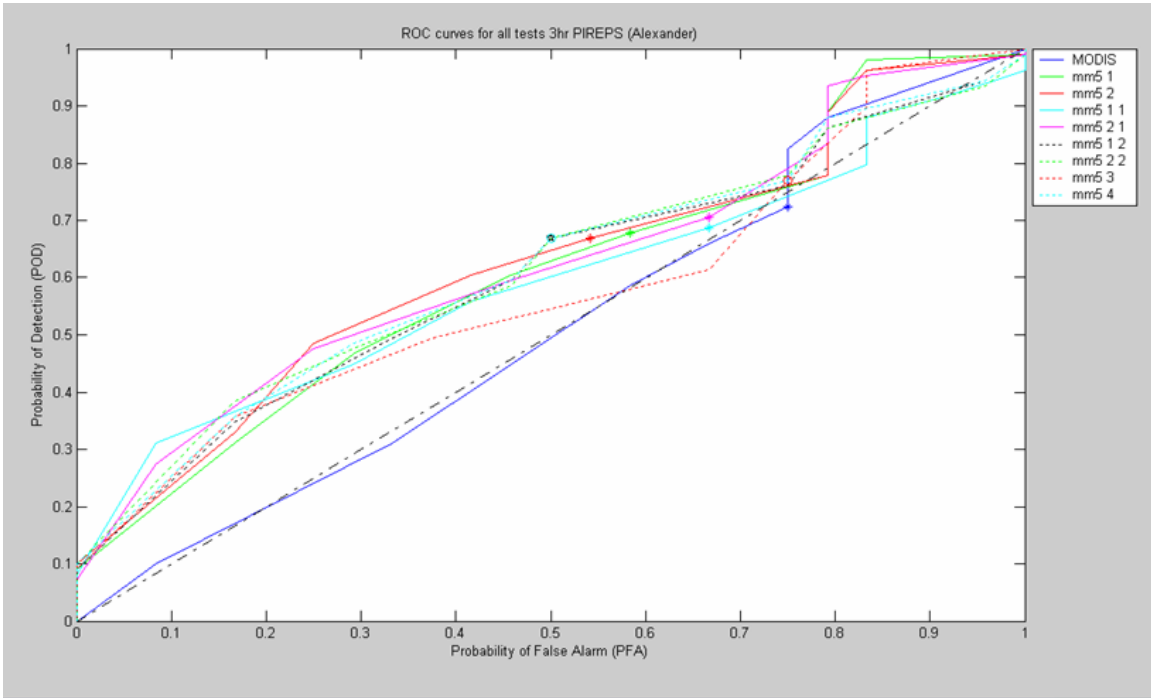


Figure 25. ROC curves using 3 hour PIREPs and Alexander Tmap with symbols plotted at the 0.5 threshold values.

Figure 25 is a plot of the POD and FAF values for all of the icing potential calculations and the MODIS icing potential as the threshold is varied from zero to one. The MODIS icing potential line is the solid dark blue line, and acts as the reference for the other tests since they are expected to improve upon the MODIS algorithm. Important to note is that the MODIS algorithm falls almost directly on the one to one line, and normally this is considered to be a poor test. It is easy to see that the addition of model data using the Alexander Tmap improved upon the MODIS algorithm in every case except possibly the MM5\_3 test. It can also be seen that at the 0.5 threshold value (values marked by the symbols) the MM5\_1\_2, MM5\_2\_2, and MM5\_4 tests plot furthest to the top and left indicating that these tests performed the best. It should be noted that the jagged nature of the test curves in the upper right portion of the graphs is likely due to the limited number of negative icing PIREPs.

As stated previously, some believe it is inappropriate to use the FAF and POD as a measure of algorithm success. Since FAF is simply  $1 - \text{POD}_{no}$ , it is also an indicator of  $\text{POD}_{no}$ . With that in mind it also seems inappropriate to

ignore the results found in Table 4 and Figure 25, where at the 0.5 threshold, there is a 0.05 drop in POD and a 0.25 increase in PODno over the MODIS algorithm alone using the MM5\_1\_2 calculation. Using the AE measure alone would completely miss the fact that there was a 100% increase in PODno percentage with only a 7% drop in POD. This would indicate that including the model data in an area limited by the horizontal extent of the MODIS algorithm could greatly increase efficiency. This finding could be missed if POD and PODno were looked at only separately.

The ROC curves produced using the CIP Tmap can be seen in Figure 26. This case looks quite different than the Alexander Tmap case. The MODIS icing potential line is again the solid dark blue line, and acts as the reference for the other tests. Again, the MODIS algorithm line falls almost directly on the one to one line since it is the same plot seen in the Alexander Tmap ROC curves. Here the addition of model data it does not add as much value, and in cases actually reduces the value. This can clearly be seen at the 0.5 threshold value, where only three of the tests fall above, and to the left, of the one to one line, and four actually fall below and to the right. As possibly expected, the three tests that plot furthest to the top and left at the 0.5 threshold are the MM5\_1\_2, MM5\_2\_2, and the MM5\_4.

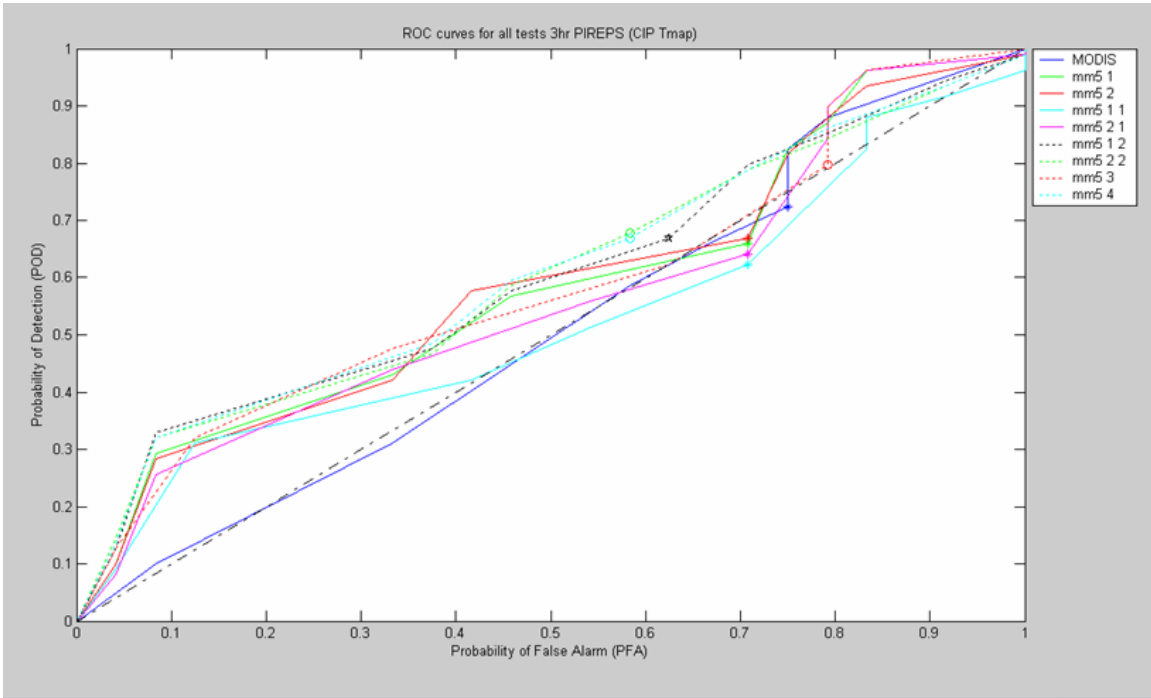


Figure 26. ROC curves using 3 hour PIREPs and Alexander Tmap with symbols plotted at the 0.5 threshold values.

## V. CONCLUSION AND RECOMMENDATIONS

### A. CONCLUSION

The Alexander (2005) MODIS based daytime icing potential algorithm provided a unique opportunity to examine the benefits of adding mesoscale model data to the icing potential calculations. The two dimensional nature of satellite based icing potential products severely limits their operational use as a stand alone product, but they are extremely helpful in limiting the horizontal extent of diagnosed icing. In the past, icing products that were strictly based on model data fields greatly over predicted the extent of high icing potential, which makes the combination of these two products highly beneficial.

The first conclusion that one must come to when reviewing the result in chapter IV is that the CIP Tmap is far too temperature dependant. As seen in Figure 6, the CIP Tmap has a broad range of temperatures (-8 through -4 degrees Celsius) that assign a maximum icing potential. This is compared to the Alexander channel 31 brightness temperature Tmap which has a distinct peak at -10 degrees Celsius. The CIP Tmap's broad range of high icing potential did little to increase the POD values, and severely limited the total icing potential's ability to detect negative icing PIREPs. This could be due to forecasters' desire to error on the side of high icing potential in operational products, but the CIP Tmap failed to increase POD in this study and drove 4 out of 8 test ROC curves below and to the right of the one to one line. Of the remaining 4 tests only three plotted above and to the left of the one to one line, and this only occurred in model icing potential calculations that weighted T lower than RH. By comparison, the Alexander Tmap based icing potential ROC curves all plotted above and to the left of the one to one line at the 0.5 threshold. This result suggests that the CIP Tmap actually makes it more difficult to correctly detect icing, and no icing, potential. Total icing potential calculations based on the Alexander Tmap clearly performed better.

Model icing potential calculations that weighted RH values higher than T values produced more accurate results. This is likely due to the tendency of models to over predict areas of high RH, which would lead one to conclude that when a model predicts low RH it is most likely the case. This could also be due to the fact that temperatures at some altitude over any point on earth will produce a high icing potential based on T alone, but icing very rarely occurs outside of cloud or precipitation. By weighting the RH potential values higher, PODno values were elevated, which in turn moved the PFA values lower at the 0.5 threshold for icing potential. The net effect was that the MM5\_1\_2, MM5\_2\_2, and MM5\_4 ROC lines moved farther from the one to one line, and plotted farthest to the top and left at the desired threshold in both the CIP and Alexander Tmap ROC curves.

The addition of MM5 mesoscale model data added significant value to the stand alone MODIS based icing potential algorithm which bodes well for future operational products based on Alexander (2005). This type of product is not currently feasible due to the time resolution issues associated with the MODIS platform, but future GOES imagers will have similar channels and resolutions to the MODIS platform with the capability to scan the continental United States every five minutes (Allen 2006). This platform will provide a legitimate opportunity to produce a near real time icing potential field that could be viewed on cockpit displays.

## **B. RECOMMENDATIONS**

It is highly recommended that a study be conducted into the value of the CIP's operational Tmap. The results here seem to indicate that this Tmap severely limits the overall ability to detect negative icing areas, which indicated that it over predicts the high icing area. If the objective of the CIP is to accurately portray the icing potential, then the Tmap should be adjusted. The results of such a study could immediately impact the accuracy of an operational product.

As a direct follow-on to this work, it is recommended that a study should be conducted using model volume data. This would add a third dimension to the MODIS based algorithm, and the inclusion of new parameters such as cloud

liquid water content could make the model based calculations even more precise. This, along with the use of the MODIS cloud mask would provide an advance in MODIS based icing and no icing potential prediction. This study would be time and processor intensive due to the large amount of data used, but would be worth the time and effort. A large pool of both positive and negative PIREPs would aid in validation and certainty of results. While positive icing PIREPS are readily available, negative icing PIREPs are hard to come by in large numbers. To gain this data, coordination with air traffic control (ATC) may be necessary. ATC controllers could be asked to query aircraft for icing PIREPs during periods when pilots don't feel the need to provide one. This would greatly increase the probability of receiving a negative icing PIREP, and bring the number of negative icing PIREPs closer to the number of positive icing PIREPs which would smooth out ROC curves and make comparisons easier. The difficulty would be in coordinating a day when an extra tropical system is transiting an area of interest.

Finally, outside of using the MODIS cloud mask to reduce the area explored for icing, a reexamination at the entire algorithm may be in order. A large amount of time was spent looking at the various test fields produced by MODIS icing algorithm during this study, and the final group 1 icing potential field appeared ineffective. Group 1 was comprised of 5 separate tests, but the final Group 1 field could have been accurately approximated by giving every pixel in the Group 1 field a maximum icing potential value. There also seemed to be repetition in the Group 2 and 4 tests that may, or may not, add value to the over all algorithm. It may be prudent to conduct this analysis prior to conducting the larger model volume study suggested above.



THIS PAGE INTENTIONALLY LEFT BLANK

## LIST OF REFERENCES

- Air Safety Foundation, 2002: Safety Advisor, Weather No. 1: Aircraft Icing. Federal Aviation Administration. [Available online at <http://www.aopa.org/asf/publications/sa11.pdf>], accessed 19 March 2006.
- Alexander, J., 2005: Enhancement of the Daytime GOES-Based Aircraft Icing Potential Algorithm using MODIS. M.S. thesis, Dept. of Meteorology, Naval Postgraduate School, 86 pp. . [Available from Dudley-Knox Library, Naval Postgraduate School, 411 Dyer Rd., Monterey, CA 93943].
- Aviation Weather Center Aviation Digital Data Service, cited 2006: Aviation Weather Center Aviation Digital Data Service: PIREP request form, [Available online at <http://adds.aviationweather.gov/pireps/>], accessed 20 March 2006.
- Baum, B., P. Soulen, K. Strabala, M. King, S. Ackerman, W. Menzel, and P. Yang, 2000: Remote sensing of cloud properties using MODIS airborne simulator imagery during SUCCESS 2. Cloud thermodynamic phase. *J. Geophys. Res.*, **105**, No. D9, 11781–11792.
- Bernstein, B., F. McDonough, M. Politovich, B. Brown, T. Ratvasky, D. Miller, C. Wolff, G. Cuning, 2005: Current Icing Potential: Algorithm Description and Comparison with Aircraft Observations. *J. Appl Meteor.*, **44**, 969–997.
- Broeren, A., M. Bragg, H. Addy Jr., 2004: Effects of Intercycle Ice Accretion on Airfoil Performance. *J. Aircraft.*, **41**, 165–174.
- Brown, B., G. Thompson, R. Brintjes, R. Bullock, and T. Kane, 1997: Intercomparison of In-Flight Icing Algorithms. Part II: Statistical Verification Results. *Wea. Forecasting*. **12**, 890-914.
- Civil Aviation Authority, 2000. Aircraft Icing Handbook [Available online at [http://www.caa.govt.nz/fulltext/safety\\_booklets/aircraft\\_icing\\_handbook.pdf](http://www.caa.govt.nz/fulltext/safety_booklets/aircraft_icing_handbook.pdf)], accessed 19 March 2006.
- Curry, J. and G. Liu, 1992: Assessment of Aircraft Icing Potential Using Satellite Data. *J. Appl. Meteor.*, **31**, 605–621.
- Ellrod, G., J. Nelson III, 1996: Remote Sensing of Aircraft Icing Regions Using GOES Multispectral Imager Data. *AMS Weather and Forecasting Conference paper*. [Available online at <http://www.orbit.nesdis.noaa.gov/smcd/opdb/aviation/icg.html>], accessed 15 December 2004.

Erickson, S. (1997) Air line pilots. *NASA–LeRC/ CRREL/FAA Inflight Remote Sensing Icing Avoidance Workshop, Summaries and Presentations*, 1–2 April, Ohio Aerospace Institute, Cleveland, Ohio.

Fly Light Aviation Meteorology, cited 2005: Airframe and Engine Icing. [Available online at <http://www.auf.asn.au/meteorology/section10.html>], accessed January 2006.

Icing Branch-NASA Glenn Research Center, cited 2006: the Icing Branch. [Available online at <http://icebox.grc.nasa.gov>], accessed 19 March 2006.

Inoue, T., 1987: A Cloud Type Classification with NOAA-7 split-window measurements. *J. Geophys. Res.*, **92**, 3991-3999.

International Air Transport Association, cited 2006: Pressroom. [Available online at [http://www.iata.org/pressroom/industry\\_facts/stats/2005-10-31-03.htm](http://www.iata.org/pressroom/industry_facts/stats/2005-10-31-03.htm)], accessed 23 March 2006.

Kidder, S.Q. and T.H. Vonder Haar, 1995: *Satellite Meteorology: An Introduction*. Academic Press, 466 pp.

Meteorology Education & Training, cited 2006: Forecasting Aviation Icing: Type and Severity. [Available online at <http://meted.ucar.edu/icing/pcu6/>] accessed November 2005.

Meteorology Education & Training, cited 2006: Forecasting Aviation Icing: Type and Severity. [Available online at <http://meted.ucar.edu/icing/pcu62/pcu621>] accessed November 2005.

MODIS Data Support – National Aeronautics and Space Administration, cited 2006: MODIS Data Support: multiple MODIS data ordering page. [Available online at [http://daac.gsfc.nasa.gov/daac-bin/MODIS/Data\\_order.pl?PRINT=1](http://daac.gsfc.nasa.gov/daac-bin/MODIS/Data_order.pl?PRINT=1)], accessed 20 March 2006.

MODIS Web – NASA/Goddard Space Flight Center, cited 2006: MODIS Web: About MODIS. [Available online at <http://modis.gsfc.nasa.gov/about/specifications.php>], accessed 31 January 2006.

Nasiri, S., cited 2006: MODIS FILE READERS AND ACCESSORIES, Shaima Nasiri Ph.D. Research Page. [Available online at: <http://www.ssec.wisc.edu/~shaima/Matlab/MfilesOther/index.html>], accessed 19 March 2006.

National Weather Service Birmingham, AL, cited 2006: Relative Humidity Equation. [Available online at <http://www.srh.noaa.gov/bmx/tables/rh.html>], accessed 23 March 2006.

- Pavolonis, M. and A. Heidinger, 2004: Daytime Cloud Overlap Detection from AVHRR and VIIRS. *J. Appl. Met.*, **43**, 762–778.
- Planecrashinfo.com, cited 2006: Cockpit Voice Recording Transcript, [Available online at <http://www.planecrashinfo.com/cvr941031.htm>], accessed 23 March 2006.
- Politovich, M., 2003: Predicting in-Flight Aircraft Icing Intensity. *J. Aircraft*, **40**, 639–644.
- Sand, W., W. Cooper, M. Politovich, and D. Veal, 1984: Icing conditions encountered by a research aircraft. *J. Climate Appl. Meteor.*, **23**, 1427–1440.
- Sandel.com, cited 2006: Sandel SN4500 brochure, [available online at [http://www.sandel.com/Sandel\\_SN4500\\_EHSI\\_brochure.pdf](http://www.sandel.com/Sandel_SN4500_EHSI_brochure.pdf)], accessed 28 March 2006.
- Strabala, K., S. Ackerman, and W. Menzel, 1994: Cloud Properties Inferred from 8-12 $\mu$ m Data. *J. Appl. Meteor.*, **33**, 212–229.
- Tafferner A., T. Hauf, C. Leifeld, T. Hafner, H Leykauf, U. Voigt, 2003: ADWICW: Advanced Diagnosis and Warning System for Aircraft Icing Environments. *Wea. Forecasting*, **18**, 184–203.
- The National Center for Atmospheric Research & The UCAR office of Programs, cited 2006: Airplane Icing. [Available online at <http://www.ucar.edu/research/society/icing.shtml>], accessed January 2006.
- Tremblay A., A. Glazer, 2000: An Improved Modeling Scheme for Freezing Precipitation Forecasts. *Mon. Wea. Rev.*, **128**, 1289–1308.
- Thompson, G., R. Bullock, and T. Lee, 1997a: Using Satellite Data to Reduce Spatial Extent of Diagnosed Icing. *Wea. Forecasting*, **12**, 185-186.
- Thompson, G., R. Brientjes, B. Brown, F. Hage, 1997b: Intercomparison of In-Flight Icing Algorithms. Part I: WISP94 Real-Time Icing Prediction and Evaluation Program. *Wea. Forecasting*, **12**, 878–889.
- Wieman, S., 1990: *Multiple Channel Satellite Analysis of Cirrus*. M.S. thesis, Dept. of Meteorology, Naval Postgraduate School, 60pp.
- Young, S., C. Platt, R. Austin, and G. Patterson, 2000: Optical Properties and Phase of Some Midlatitude, Midlevel Clouds in ECLIPS. *J. Appl. Meteor.*, **39**, 135–152.

THIS PAGE INTENTIONALLY LEFT BLANK

## INITIAL DISTRIBUTION LIST

1. Defense Technical Information Center  
Ft. Belvoir, Virginia
2. Dudley Knox Library  
Naval Postgraduate School  
Monterey, California
3. Philip Durkee  
Naval Postgraduate School  
Monterey, California
4. Carlyle Wash  
Naval Postgraduate School  
Monterey, California